

Structural characterisation of MscM and
investigation of protein-lipid dynamics of
MscS in MSP1E3D1 nanodisc

Meenakshi Anil

27.11.2022

Table of contents:

Abstract	8
Chapter 1: Introduction to Mechanosensation.....	9
1.1 Bacterial mechanosensitive ion channels	9
1.1.1 MscS-like family	10
1.1.2 MscS	11
1.1.3 MscL	12
1.1.4 MscM	13
1.2 Mechanosensitive ion channels across nature	14
1.2.1 Roles in infection	14
1.2.2 Roles in osmotic regulation	13
1.2.3 Roles in carnivorous plants	14
1.3 Role of the local environment in mechanosensation	15
1.4 Techniques widely used to investigate MS channels	17
1.4.1 Electron paramagnetic resonance spectroscopy.....	17
1.4.2 Nuclear magnetic resonance spectroscopy	18
1.4.3 Cryogenic electron microscopy	19
1.4.4 X-Ray crystallography	20
1.4.5 Liposomes	19
1.4.6 Nanodiscs	19
1.4.7 AlphaFold models	20
1.4.8 Molecular dynamics simulations of protein-lipid dynamics	22
1.5 Project aims and hypothesis	24
Chapter 2: Materials and Methods	25
2.1 Materials	25
2.1.1 Table of materials	25
2.1.2 Buffers composition	27

2.1.3 Oligonucleotides	28
2.2 Methods	29
2.2.1 PCR	29
2.2.2 Transformation to bacterial cells for genotype sequencing	29
2.2.3 Overnight cultures	30
2.2.4 Miniprep	30
2.2.5 Plasmid sequencing	30
2.2.6 Plasmid transformation	30
2.2.7 Cell culture and protein purification	31
2.2.7.1 Cell growth	31
2.2.7.2 Membrane protein purification	31
2.2.7.3 cwEPR measurements.....	32
2.2.7.4 Imidazole gradient optimisation.....	33
2.2.8 Preparing lipids for reconstitution experiments	34
2.2.9 SapA nanodisc reconstitution	34
2.2.10 SapA nanodisc reconstitution optimisation	35
2.2.11 Liposome reconstitution	35
2.2.12 Molecular Dynamics simulation	36
Chapter 3: Results and Discussion - Experimental and computational investigation of MscS-like channels	37
3.1 Dynamics of MscM gating by PELDOR and AlphaFold	38
3.1.1 MscM purification	39
3.1.2 Imidazole gradient optimisation	41
3.1.3 MscM in detergent	43
3.1.4 Reconstitution of MscM in lipid environments	45
3.1.4.1 SapA nanodisc reconstitution	45
3.1.4.2 Liposome reconstitution	48

3.2 MscS in MSP1E3D1 nanodisc	51
Conclusion	56
References	57

Abbreviations

AA	All-atom
CG	Coarse-grained
CryoEM	Cryogenic electron microscopy
cwEPR	Continuous wave- electron paramagnetic resonance spectroscopy
DDM	n-Dodecyl-beta-Maltoside
DNA	Deoxyribonucleic acid
DOPC	1,2-Dioleoyl-sn-glycero-3-phosphocholine
EPR	Electron paramagnetic resonance spectroscopy
IMAC	Immobilized metal affinity chromatography
IPTG	Isopropyl beta-D-1-thiogalactopyranoside
kDa	Kilo Dalton
LB	Luria Bertani Medium
MD	Molecular dynamics
MS	Mechanosensitive
MTSSL / MTSL	Methyl methanesulfonylthioate
Ni-NTA	Ni ²⁺ -Nitrilotriacetic acid

NMR	Nuclear magnetic resonance spectroscopy
NP	Nanopocket
N-terminus	Amino terminus
OD	Optical density
PAGE	Polyacrylamide gel electrophoresis
PBS	Phosphate buffer solution
PCR	Polymerase chain reaction
PELDOR	Pulsed electron-electron double resonance spectroscopy
SDS	Sodium dodecyl sulfate
TCEP-HCl	Tris (2-carboxyethyl) phosphine hydrochloride

Acknowledgement

I would like to thank the members of the Pliotas Lab for the support during my master's programme, my supervisor - Dr Christos Pliotas, Dr Theodoros Karamanos, Bolin Wang, Benjamin Lane, Yue Ma, Katie Hardman, Nana Yan, Dr Emily Wheeler, and Dr Mariangela Dionysopoulou.

Author's declaration

I declare that this thesis has been generated by myself and the work completed during the project was completed by myself with the guidance and supervision of members of the Pliotas Lab, except where indicated otherwise.

Abstract:

Cell membranes play significant role in cells for the regulation of entry and exit of molecules.

The cell membrane is comprised of lipids and integral membrane proteins.

Mechanosensitive ion (MS) channels are membrane proteins that sense mechanical force and produce electrochemical information. These channels are seen across all forms of life, playing a vital role in the survival of some organisms. Bacterial MS channels, particularly *Escherichia coli* MscS and MscL, are extensively studied for the structure, function, and kinetics of these channels. MscM of the MscS-like family has an unresolved structure. This thesis covers a novel approach at resolving the structure of MscM. The approach is a curation of state-of-art techniques such as AlphaFold models, PELDOR and MD simulations, to resolve the structure of MscM. To further investigate the structural characterisation of MscM, we conducted experiments in detergent and lipid environment conditions. We have observed changes in cwEPR spectra of samples in different conditions. Additionally, the protein-lipid dynamics of MscS within a membrane mimetic system was investigated using MD simulations.

Chapter 1: Introduction to mechanosensation

Cell membranes of living organisms are essential for the survival and functioning of all organisms. They are mainly constituted of lipid molecules and membrane proteins. The polar lipid bilayer forms a barrier and regulates the entry and exit of molecules associated with the cell function. Protein-lipid interactions are seen to have vital roles in maintaining membrane protein structure and function. Mechanosensitive (MS) ion channels are integral membrane proteins that respond to mechanical stimuli, by transducing mechanical force into intracellular biochemical or electrical signals [1]. MS ion channels have a central pore that allows the transport of selected ions and solutes into and out of the cells in response to membrane tension. Mechanotransduction can be seen across all living organisms and play significant roles in survival for organisms like bacteria. In prokaryotes, MS channels act as pressure safety valves to protect bacterial cells from rupturing during hypoosmotic shock [2]. In eukaryotes, they play a role in various physiological processes including proprioception, pain sensation, hearing, micturition, cell volume regulation and cardiovascular processes [3]. Abnormal MS channel function can lead to cardiac arrhythmias, neuronal and muscular degeneration [3]. In plants, MS channels play a role in various aspects: pollen tube growth, lateral root emergence [4], osmotic stress, gravity responses, etc. [5]. In fungi, during hypoosmotic conditions, MS channels maintain intracellular Ca^{2+} and cell volume for survival [6]. In filamentous fungi, MS channels overexpression showed increased CaCl_2 toxicity or/and reduced formation of asexual spores [7].

This chapter provides a background on MS channels and the roles played by them across nature. The chapter also broadly discusses some experimental and computational approaches used to investigate the protein-function-dynamic triad of these complex but fascinating membrane proteins.

1.1 Bacterial mechanosensitive ion channels

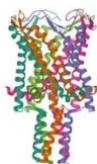


MS ion channels were first identified in *Escherichia coli* (*E. coli*) using the patch-clamp electrophysiology method. MS channels are categorised based on their conductance at

different membrane potentials. Channels with conductance 1nS are called MscS – (MS channels small conductance), they are weakly selective for anions [8].

Channels of 3nS conductance are called MscL – (MS channel large conductance), they are nonselective pores [8] and MscM – (MS channels mini conductance) with a conductance of 0.3nS [9]. The selectivity of MscM is not known yet. MscS and MscL are best characterised and studied in *E. coli* [10]. Structures in various conformational states for both the channels have been elucidated and their gating mechanisms have been extensively studied. Their primary function in *E. coli* is to act as emergency pressure safety valves to protect cells from rupturing due to excessive turgor [2]. In a condition of osmotic down shock, the pressure across the cell membrane increases, activating the MS channels to open and release metabolites from the cell, to ensure its survival [11].

1.1.1 MscS-like family

E. coli has six MscS family members: MscS, MscK, YbdG, YnaI, YbiO and MscM (Table 1). The crystal structures of MscS in different conformational states have been elucidated [12] and recently, the structures of YnaI and YbiO were obtained using CryoEM [13]. YnaI, YbdG and MscS have 5 transmembrane (TM) helices, whereas YbiO and MscM comprises of 11 TM helices and extensive periplasmic domains [10]. MscK and YbdG play a minor role in cell integrity maintenance [10]. MscK is a K⁺ regulated channel, encoded by *kefA* which is homologous to the *yggB* which encodes MscS activity [14]. One of the main components of MscM is *yjeP*, overexpression of *YjeP* promotes survival in the absence of all other MS channels [10]. YbdG knockout mutants showed slight defect in osmotic shock survival [15]. Further investigation is required to get an insight on the distribution and function of the different family members within the membrane, and to observe any co-dependence among the channels.

Channel	MscL	MscS	YnaI	YbiO	YbdG	MscM	MscK
Structure				Partial structure	Unknown	Unknown	Unknown

Polymer	Pentamer	Heptamer					
Size (kDa)	75	210	280	580	329	875	900
TM diameter (Å)	55	75	95	170	120	190	200
No. of TM helices	10	21	35	70	35	77	84
Conductance (nS)	~3	~1	~0.1	~1	~0.4	~0.3	~0.8
Pressure activation threshold (mN/m)	10-15	5-8	~10	~10	~5	~7	~6

Table 1: MscL and MscS-like channels. Details of the MscS and MscS-like channels [9] [10] [13] [16].

1.1.2 MscS

E. coli MscS is a 286 amino acid homoheptamer, consists of seven identical subunits aligned to form a central pore. Each monomer consists of three transmembrane (TM) helices. TM1 and TM2 form sensor paddles, tilted away from the channel axis [17]. TM3 has a kink at G113, which was initially thought to be the cytoplasmic boundary [18]. The N-terminal half - TM3a, forms the pore-lining helix whereas the C-terminus end - TM3b, is predicted to be between lipids and the cytosol, spanning parallel to the membrane. TM3a helices form a hydrophobic seal in the closed conformational state of the channel [2]. Structure of MscS embedded in nanodisc (MscS-ND) resemble the crystal structures obtained of structures solubilised in detergent micelles. The arrangement of helices TM2 and TM3a were proposed to be partially embedded in the cytosolic leaflet of the membrane and only TM1 extends to the periplasmatic side of the membrane (Fig. 1) [17]. The paddles – TM1 and TM2, tilt 18° more with respect to the membrane normal during closed-to-open transition, changing the diameter of the pore from 5 to 14Å. The pore of MscS is majorly apolar except for the NH2-terminus Ser95 of TM3. The transmembrane domain of MscS has a positive electrostatic potential due to the abundance of arginines in the membrane-spanning helices. The weakly

selective nature of MscS for anions over cations could be due to the electrostatic effects [18]. In response to mechanical stimuli, repositioning of the arginines embedded in the membrane would rearrange the helices and change cross-sectional area of *E. coli* MscS, required for mechanosensitivity [18].

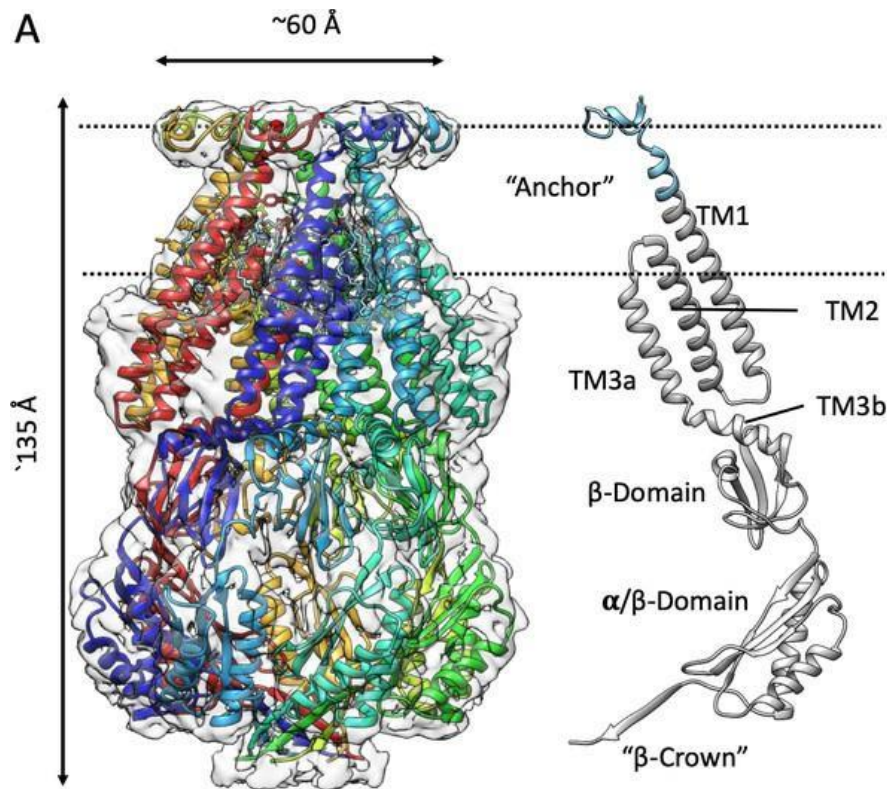


Figure 1: Structure of MscS reconstituted into a nanodisc [17]. The 3.1 \AA resolution heptameric structure is shown on the left side, each monomer is represented by a different colour. Lipids bound to the protein are visualised using stick representation. The figure on the right panel shows an individual monomer of MscS. The cyan regions were the regions resolved in the MscS-ND structure. The pair of dotted lines show the presumed region of the lipid bilayer.

1.1.3 MscL

The first MS ion channel to be cloned was *E. coli* MscL (EcMscL). Sukharev et al., studied the functional characteristics of MscL using liposome-reconstituted fractions and patch-clamp electrophysiology [19]. Significant differences were seen in hypotonic-shock-induced

membrane permeability between a *mscL* knock-out mutant and wild type strains. They proposed that MscL is required and is adequate for mechanosensitivity [19].

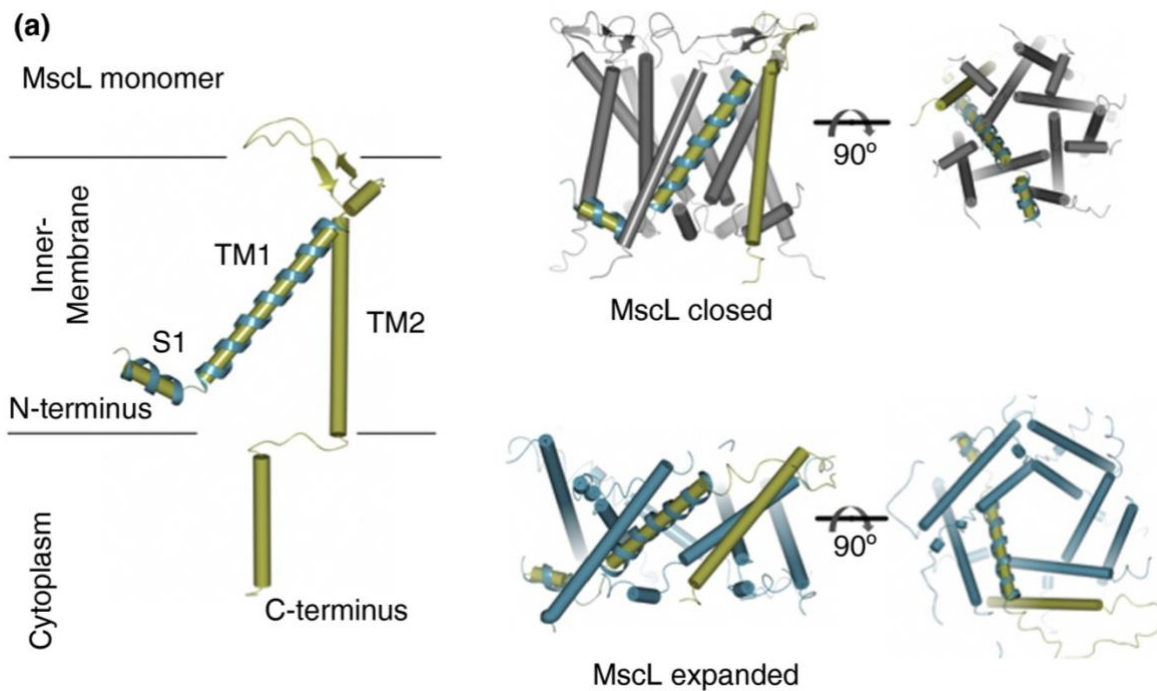


Figure 2: MaMscL model in closed and open states. By comparing crystal structures, changes in orientation of TM helices is observed during gating of the channel in response to membrane tension [20] [21].

Structures of EcMscL orthologues from *Mycobacterium tuberculosis* (TbMscL) and archaeal *Methanosarcina acetivorans* (MaMscL) have been resolved in detergent. TbMscL and EcMscL show high similarity between their amino acid sequences [22]. TM1 of TbMscL spans the membrane which forms the bulk of the pore. TM1 of MscL is highly conserved among bacterial species, suggesting significance of the domain in channel function. A study using patch-clamp experiments reported that single residue substitutions affected kinetics of the channels. Residues in the periplasmic region (Q56 and K31) when substituted caused change in the gating of the channel [23]. Crystal structures of MaMscL in closed and expanded state gave an insight into the movement of transmembrane helices. MaMscL TMs 1 and 2 outward towards the plane of the membrane was observed in response to membrane tension (Fig. 2) [20] [21] [24].

1.1.4 MscM

MscM – MS channel of miniconductance activity has a conductance of $\sim 0.300\text{nS}$ [9]. Cells are protected from hypoosmotic shock when yjeP is overexpressed. Initially, MscM was proposed to be comprised of multiple channel components like YbdG. MscM channel activity was observed in null mutations of YbdG, suggesting that MscM activity could not be attributed to YbdG alone [10]. yjeP is on an operon with phosphatidylserine decarboxylase (PSD), the gene codes for a significant enzyme that converts phosphatidylserine to phosphatidylethanolamine. The alternative sigma factor, σ^E and two component system regulator, CpxAR control the expression of the operon with yjeP and psd. Both, σ^E and CpxAR respond to extracytoplasmic stress. It is proposed that while PSD is necessary to maintain the integrity of inner and outer membranes, under conditions of stress, MscM may be activated to modulate turgor [10].

1.2 Mechanosensitive ion channels across nature

1.2.1 Roles in infection

Mutations of YbiO have been linked to pathogenicity. A single glycine to arginine mutation in the YbiO gene has been associated with *Salmonella* infections [25]. Egg whites have conditions that are not suitable for bacterial survival in terms of pH and nutritional environment, whereas the egg yolk is seen to have conditions appropriate for *Salmonella enteritidis* growth. *Salmonella enteritidis* contamination is largely dependent on the movement of the bacterial cells from the egg white to the egg yolk. Strains of *Salmonella enteritidis* are seen to have varied capabilities of survival in egg whites. A 120-base pair deletion was identified in ybiO gene of a strain of *Salmonella enteritidis* studied by Wang et al [26]. Further studies are required to understand the role played by YbiO, an MS channel, in altering the survival abilities of *Salmonella enteritidis*.

1.2.2 Roles in osmotic regulation

In humans, mechanically activated ion channels are known to play various roles in physiology and pathophysiology. Some of the transient receptor potential channels (TRP) are a family of channels that are activated by mechanical stimuli. TRPV4 is a member of the family that has been extensively studied. TRPV4 is observed to be activated by hypotonic

stress; there have been models suggesting the channel could be directly or indirectly mechanically gated. The molecular mechanisms for the activation of the channel are not fully understood [27]. TRPV4 is expressed abundantly in different types of cells – epithelial cells, smooth muscle cells and immune cells [28].

TRPV4 has been shown to play a role in osmotic sensing in mice, TRPV4 knockout mice were shown to have impaired osmotic regulation [29]. The water consumption and levels of antidiuretic hormone were lower in the knockout mice. The findings of the study suggested that TRPV4 is a requirement for normal systemic osmotic homeostasis [29].

1.2.3 Roles in carnivorous plants

The carnivorous plant *Dionaea muscipula* (Venus flytrap) from the *Droseraceae* family, and the sensitive *Mimosa pudica* exhibit mechanosensitive activity. The Venus flytrap traps its prey when their mechanosensory trigger hairs are deflected. The FLYC1 gene is proposed to be the gene localised to the mechanosensory cells in trigger hairs. Stretch-activated chloride currents were seen when FLYC1 was overexpressed in Human Embryonic Kidney (HEK) – mechanically insensitive cells. This result suggests that FLYC1 encodes an MS ion channel [30]. Another carnivorous plant, the *Drosera capensis* (Cape Sundew) from the same *Droseraceae* family, is seen to have highly enriched transcripts of FLYC1 homologs in the sensory tentacle of the species [30].

1.3 Role of the local environment in mechanosensation

Significant work has been done to investigate the mechanisms of MS channel gating. The bilayer model suggests that membrane tension can activate MS channels through surrounding amphipaths [31]. The membrane bilayer is majorly formed by lipid molecules. Lipids are amphipathic molecules that show both hydrophobic and hydrophilic character [31]. The significant role of lipids in the gating of MS channels has been widely accepted as the ‘lipid-moves-first’ model proposed by Pliotas et. al., [2]. Studies have combined experimental approaches to investigate the gating of MS channels with regard to the pressure changes within the bilayer.

Through molecular dynamics simulations and biophysical analyses studies of MscS, it has been identified that ‘pockets’ or ‘voids’ are formed by the arrangement of TMs1 and 2 and

TMs 3a and 3b. With transition in the conformational state of the protein, the volumes of the voids change [2]. Pliotas et al., proposed that occupancy of the pocket by lipids determine the conformational state of MscS. Under membrane tension, exchange of lipids between the protein pockets and lipid bilayer destabilises the closed structure of MscS; transitioning to the open state with less lipids as the pockets have less volume [2]. The study ran repeated multiscale simulations and observed lipid migration to protein voids, also reported that most lipids occupied the top half of the pockets. During transition, the number of lipids within pockets reduce to one lipid per pocket [2]. The lipids that exit during transition were observed to be between TMs 2 and 3a.

The structure of MscS reconstituted into a nanodisc resolved by Rasmussen and colleagues, to determine the structure in lipid environment observed protein-lipid interaction—per subunit, three phospholipid molecules were observed [17]. Two of the phospholipids observed within the pocket, were parallel to TM3b, one of them formed a salt bridge with R59. The best resolved lipid was near the periplasmic side, the head group formed a strong salt bridge with R88 at a loop between TM2 and TM3a. Densities were also reported within the pore which could be phospholipid molecules from the periplasmic side, obstructing the central pore. An R88W mutation was introduced that destabilised the salt bridge interaction; this increased the pressure required for channel opening. A loss-of-function phenotype was observed with the R88W MscS mutant in electrophysiology experiments [17]. Introduction of a hydrophobic R59L mutation in the pocket region, has been shown in another study, to disrupt the salt bridge and allow easy lipid removal from the pocket, thereby affecting tension sensing of the channel in a gain-of-function phenotype [32].

In a recent study by Zhang et al. [33], that aimed to visualise MscS under membrane tension with the use of nanodiscs, they classified lipids seen in molecular dynamics simulations as ‘pore’, ‘gatekeeper’ and ‘pocket’ lipids. Molecular dynamics simulations of MscS in different states were performed. It was observed that pore lipids were stable and needed for MscS to be impermeable in the closed state. The group also observed that lipids moved rapidly to the periphery of the pore in the open state, allowing ion permeation [33]. Gatekeeper lipids are positioned in a hydrophobic pocket between two adjacent subunits extending into solvent-exposed region of MscS. This pocket was seen to be occupied by a density,

consistent with lipid molecules in closed state maps. This lipid is assumed to be a significant factor in MscS mechanosensation. Under membrane tension, when the gatekeeper lipid dissociates from MscS, TM1-TM2 show increased mobility and the closed state of the channel gets disrupted. Once the lipid interaction with the binding pocket is lost, it cannot associate in the same orientation as earlier, leading the channel to change to an open conformation [33]. Sustained membrane tension leads to increasing number of lipid removal from MS channel nanopockets, causing tension-induced conformational changes and therefore, MS channel gating [33].

A study by Wang et al., investigated MscL channel gating by comparing MscL states in the absence of tension and after pocket delipidation. They reported that tension could be imitated by modifications within the pocket region, and this could interrupt the lipid pathway between the bulk bilayer and pocket lipids [34]. They introduced a modification L89W into MscL- a tryptophan residue, that led to steric hindrance at the pocket. They compared the dynamics of WT MscL and L89W MscL under membrane tension. MD simulations showed lipids entered and occupied pockets of L89W MscL during equilibration. On application of bilayer tension on the L89W channel, that was sufficient for WT MscL channel to open, the lipids were unable to leave the pocket due to the bulky tryptophan modification. Global structural changes were seen of the L89W MscL under tension, but due to the tight interaction of the trapped lipids within the pockets, the pore could not hydrate. They provided evidence for the lipids-moves-first model, a direct consequence of lipids being stuck within pockets is that the channel pore cannot open under sufficient bilayer tension [34].

The recent 2021 Nobel Prize in Physiology or Medicine was awarded to David Julius and Ardem Patapoutian for the discovery of touch and temperature receptors. PIEZO1 and PIEZO2- MS channels that mediate sensations of touch, proprioception, etc., were identified as mechanically activated ion channels. Gene mutations in PIEZO2 have been associated with genetic disorders showing impaired sensations of proprioception, touch and vibration. PIEZO channels behave as mechanosensors in internal organs. PIEZO1 in red blood cells play a role in cell volume homeostasis in response to mechanical force [35]. Deletion of *Piezo1*, showed red blood cells overhydration. Yoda1 a chemical activator of PIEZO1 lead to

dehydration of the cells. High resolution structures of PIEZO1 [36] and PIEZO2 [37] have been solved. Studies have shown the activity of PIEZO1 was supported by allosteric interaction of a lipid-binding pocket [36]. This suggests lipids play a role in gating of mammalian PIEZO proteins. The 2021 Nobel Prize for the discovery of mechanical transducers has begun a new phase of research for the field of MS ion channels [35].

1.4 Techniques widely used to investigate MS channels

1.4.1 Electron paramagnetic resonance spectroscopy

The fundamental principle of electron paramagnetic resonance spectroscopy (EPR-spectroscopy) is based on the absorption of microwave radiation by an unpaired electron spin in a molecule. This can be measured in the presence of an external magnetic field [38]. EPR spectroscopy is widely used in structural biology to observe and characterise conformational states of membrane proteins in different conditions, such as proteins embedded within lipid bilayers. Site-directed spin labelling is a method used to introduce unpaired electrons into biological systems, in the form of nitroxide based spin-label probes. Cysteine residues are introduced at sites of interest using site-directed mutagenesis and were further reacted with spin-label probes to produce an EPR-active species. Methanethiosulfonate spin label (MTSL) is a widely used spin-label that results in a side-chain spin-label EPR-active species [38]. It is also employed in paramagnetic relaxation enhancement nuclear magnetic resonance (NMR) studies to investigate long-range distance restraints (up to $\sim 35\text{\AA}$) [39].

Conformational states of the proteins can be studied by observing the continuous wave-EPR (cwEPR) spectra of the spin-labelled side-chain of the protein. The environment of the nitroxide spin label changes the flexibility of the spin-label; the spectral lineshape is dependent on the mobility of the spin-label side-chain [38]. Information on the polarity of the neighbouring environment of the spin label, dynamics and distances between spin labelled sites within 2\AA can be retrieved using cwEPR [39] [40]. The limitation of cwEPR spectroscopy is the restraint of 2\AA inter-spin distances. Pulsed electron-electron double resonance (PELDOR) spectroscopy is used to measure larger distances between spin labels ($15\text{-}160\text{\AA}$), this is particularly useful in protein complexes with multiple subunits [41]. The

technique is powerful as it can be used for experiments of biological species in different environments [39].

1.4.2 Nuclear magnetic resonance spectroscopy

Nuclear magnetic resonance (NMR) spectroscopy is applied to determine the structure and dynamics of membrane proteins in bilayers and phospholipid assemblies. To identify atoms that are close together in space, the principle of the technique uses magnetic spin properties of atomic nuclei of molecules [42]. Some isotopes are added to protein samples to simplify NMR data by making it possible to identify isotopes and chemical groups [42]. The protein samples in solution are placed within a magnetic field and the magnetic moments of individual nuclei align with the field. Protein samples are exposed to pulses of radio frequency electromagnetic radiation and NMR-active nuclei will resonate at characteristic frequencies. The frequencies are acquired as NMR peaks and are termed as “chemical shifts”. The molecular environment determines the chemical shift of an atomic nucleus. The chemical shift will differ for each atom in a protein molecule due to their stereochemical positioning, unless two atoms are magnetically equivalent [42]. There are multiple advantages to using NMR for structural biology studies: the protein sample can be of various types – soluble detergent micelles, membrane proteins within nanodiscs, etc [43]. The key advantage of using NMR is the effectiveness of the technique with detergent-free membrane preparations, closer to the native environment of the protein. Solution NMR studies can be used to observe dynamics and functional interactions of membrane proteins at different timescales [44]. The limitations of NMR spectroscopy are that larger proteins (>50 kDa) are not commonly used for NMR as they have quicker relaxation rates, producing wider NMR peaks that can merge with each other [42]. Since proteins are assessed in solution in NMR, another limitation arises. The technique can only be effectively used for proteins that are stable in solution, that have less chances to aggregate around 1 mM concentrations [42].

1.4.3 Cryogenic electron microscopy

Cryogenic electron microscopy (cryo-EM) is carried out by flash freezing biological molecules and radiating the samples with electron beams. Flash freezing is done by loading a sample in a thin layer of vitreous state water on a grid. The EM grid is vertically immersed into a cryogenic coolant – usually ethane or an ethane-propane mixture. Vitrification eliminates two

problems associated with electron microscopy: dehydration and radiation damage. The vitrification process keeps the sample embedded in its native state and prevents dehydration of the sample. The cooling also aids in reducing the damage of the biological samples from the electron beam [45] [46]. Projection images of the samples in various orientations are recorded. 3D structures of the protein are constructed by processing two-dimensional images, using algorithms, to give almost atomic resolution structures. In traditional electron microscopy (EM), samples are prepared by chemical fixation, dehydration and staining. Whereas in cryo-EM, the native hydrated state of the biomacromolecules is maintained. The main advantages of using cryo-EM for structural biology is that crystallisation of protein sample is not required. Additional advantages of cryo-EM include the reduced damage by radiation ensuring the native and functional states of samples are preserved. The limitations of cryo-EM are that samples need to undergo freezing; this may destroy samples or may introduce contaminants during the freezing process [45].

1.4.4 X Ray Crystallography

The principle of X-ray crystallography is the exposure of crystallised biological molecules to X-ray beams to obtain a molecular structure. X-ray crystallography is widely adopted to resolve 3D structures of protein structures in high-resolution [47]. The most challenging part of X-ray crystallography is obtaining protein crystals. Developing the conditions for crystals to grow is the rate limiting step. Multiple factors must be controlled and kept under consideration for crystallisation. It is difficult to crystallise highly dynamic or flexible proteins, whereas macromolecules with high symmetry crystallise quickly [48].

1.4.5 Liposomes

Liposomes are spherical vesicles of phospholipid bilayers that mimic the native lipid bilayer systems that embed membrane proteins. Membrane proteins can be surrounded by the hydrophobic regions of the liposome while the centre of the liposome accommodates the hydrophilic regions of the protein. Liposomes are chosen for experiments due to the adaptability in the composition, size, and amphiphilic characteristics of liposomes. Liposomes are used for functional assays of membrane proteins, which allows a functional and structural study of the target proteins [49].

1.4.6 Nanodiscs

Nanodiscs are widely used in membrane protein structural biology studies to observe function and structure of membrane proteins embedded in a lipid bilayer. They are formed from the assembly of phospholipids with amphipathic helical proteins called membrane scaffold proteins (MSP) (Fig. 1) [50]. The lipid components of the nanodiscs are held in place by the MSP. Nanodisc sizes can be customised by altering the length of the MSP [51]. Nanodiscs can be used with different experimental techniques. The use of nanodiscs have several advantages: membrane proteins can be observed in their native environment in solution, lipid composition of the bilayer can be controlled, preparations of nanodiscs can be frozen with or without embedded membrane protein. Nanodiscs have been used to compare MS channel structures in detergent and in lipids [22]. Nanodisc structures have more structural stability and lifetime when compared to bicelles [52].

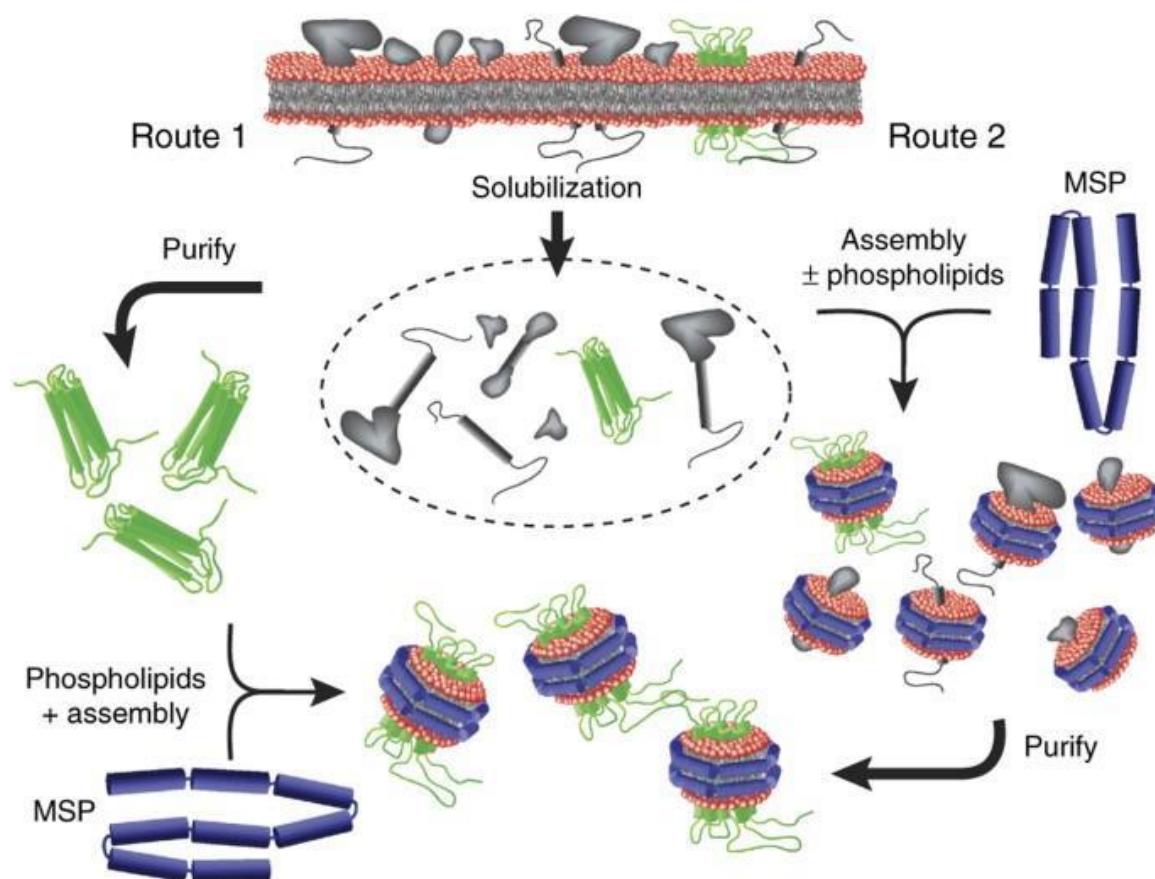


Figure 3: Nanodisc assembly [52]. The two standard methods used to assemble membrane proteins into nanodiscs. Selected membrane protein for nanodisc preparation is represented in green, and the membrane scaffold proteins (MSP) is shown in blue.

SapA nanodiscs are versatile tools for membrane protein reconstitution due to its flexibility to accommodate protein structures of different molecular weights. Additionally, they are adaptable to be used with various lipid molecules. SapA nanodiscs are extremely stable structures and can be used in different pH values and temperatures, due to high thermostability (0-95°C) [53]. Crystallisation of SapA with various lipids have been reported and a crystal structure using sulfur single-wavelength anomalous diffraction (SAD) phasing, revealed interesting features. An interesting feature of SapA-detergent complex was that no saposin-saposin interactions were seen within the complex; the assembly was held in place by hydrophobic core of the detergent [54].

1.4.7 AlphaFold Models

Determining protein structures is essential to get an insight of their function and dynamic properties. A large number of protein sequences are known but structures have been elucidated for only a minute fraction of these proteins. Computational methods have been adopted over the years to predict three-dimensional structures of a protein with the primary amino acid sequence available. Over the years, this method has largely been dependent on the existence of a resolved structure of a homologous species. AlphaFold is a computational approach that has been recently developed and can be used to predict protein structures without the requirement of a previously solved similar structure. The atomic accuracy of the method is proximate to experimental accuracy of predicting protein structures [55].

1.4.8 Molecular dynamics simulations of protein-lipid dynamics

Molecular dynamics (MD) simulations are based upon applying Newton's equations simultaneously to all atoms within a system. This allows to simulate the atoms' new positions and velocities and observe the changes in the system over the course of the simulation [56]. Molecular simulations are being increasingly used to study structure of proteins and lipid bilayer behaviour. Using molecular simulations provides insight into the dynamics of structures on different timescales. Simulations are used to complement experimental data and to gain further insight on areas where experimental barriers are present. Macroscopic details are relatively easily studied using experiments but are difficult to simulate, whereas molecular details can be easily accessed using simulations and are

more difficult in experimental settings [57]. Free energy calculations of lipid interactions, estimate time lipids bind to membrane proteins, can be calculated using molecular dynamics simulations [58].

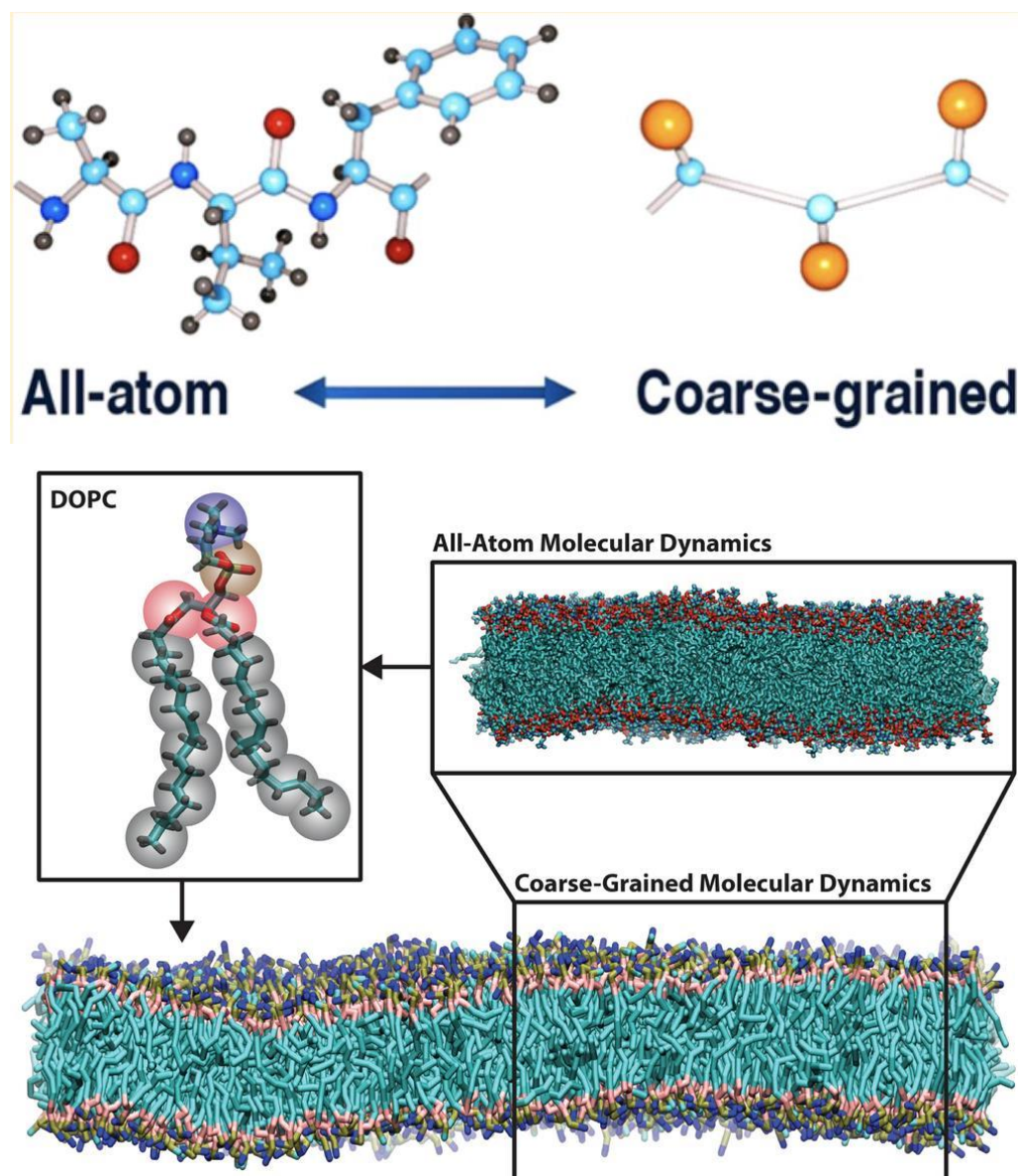


Figure 4: All-atom (AA) and coarse-grained (CG) simulation representations [59] [60]. Figure A shows the representation of a tripeptide in an atomistic model and a coarse-grained model [59]. Figure B shows the difference in representation of a DOPC lipid bilayer between a Martini coarse-grained and an all-atom simulation. The structure on the left shows a single

DOPC molecule, the coloured beads show the mapping of the molecule in a Martini coarse-grained model.

The use of simulations to observe lipid-protein dynamics has supported multiple models and provided the foundation for structural studies to be built upon. Combining different experimental and computational techniques to address scientific questions provides a holistic picture, as each approach gives different answers to the aims of the study. This chapter briefly compares two types of molecular dynamics simulations: coarse-grained (CG) and all-atom (AA) simulations (Figure 4). AA simulations follow the motions of each atom in the system. CG models use “beads” that map four atoms of the structures, replacing chemical details of the structure [57]. The interactions between the beads are defined by a set of potentials called the “force field” [60]. Timescales of biologically relevant protein dynamics or interactions are too computationally expensive to simulate using AA model, therefore, CG models are opted as an alternative [59]. Due to the lack of details, timescales of CG simulations are increased by 2-3 orders. CG simulations are increasingly being used to study protein-lipid interactions of membrane proteins with their native environment due to the longer simulation timescales when compared to atomistic simulations [59].

1.5 Project aims and hypothesis

This project was a unique curation of powerful techniques used to study MS ion channels. MscM is an ~900kDa protein with unresolved structure. Previously in the Pliotas Lab, Cryo-EM was attempted to resolve the structure of MscM; due to the dynamic regions of the protein, the technique was not successful at elucidating the structure. This project takes a novel route: EPR-directed structural derivation of MscM channel by combining PELDOR data, Alpha Fold models and MD simulations. This thesis mainly addresses the portion of the project involving membrane protein sample preparation for the former mentioned technique - PELDOR. PELDOR, Alpha fold models and the Molecular dynamics simulations were completed by collaborators and members of the Pliotas Lab. AlphaFold model of MscM was assembled by postdoctoral member -Dr Andrew Hartley, Pliotas Lab. PELDOR experiments to be completed by collaborators at University of St Andrews and subsequent Molecular Dynamics simulations to be run by Bolin Wang, Pliotas Lab.

Chapter 2: Materials and methods

2.1 Table of materials

All chemicals and reagents used for this project are for laboratory research and supplied from the respective manufacturers mentioned in the materials list. All plasmids were stored as plasmid DNA minipreps at -20°C. All bacterial strains were stored at 4°C on sealed agar plates or as 20% glycerol stock solutions at -80°C. All mutants were designed using the SnapGene® protocol and were sequenced on both strands. OriginPro®2022b was used for graphical representation of all data in this thesis.

Equipment	Source
Eppendorf Tubes	Starlab UK
PCR Tubes	Starlab UK
Falcon tubes	Appleton®
Flasks, beakers, cylinders, bottles and durans	Fisher Scientific®
Pipettes	Eppendorf Research®
Gloves	Starlab UK
Petri dishes	Thermo Fisher Scientific®
Parafilm	Fisher Scientific®
Water bath	Grant instruments Ltd
Syringes	Fisher Scientific®
Syringe filters	Fisher Scientific®
Balances	Accuris instruments Ltd
pH meters	Fisher Scientific®
PCR kit	New England Biolabs®
Plasmid miniprep kit- Qiagen	Qiagen®
QIAquick PCR purification kit - Qiagen	Qiagen®
Spectrophotometer cuvettes	Fisher Scientific®
PCR machine	Bio-Rad®
SDS-PAGE electrophoresis unit	Invitrogen

Vivaspin-2 100kDa MWCO	Sartorius®
Optima XPN-80 Ultracentrifuge:	
50.2 Ti fixed angle rotor	
SW 55 Ti swinging bucket rotor	Beckman Coulter®
Avanti J-26XP High speed JLA 8.1000 rotor	
Superose 6 columns	Cytiva®
ÄKTA	Cytiva®
Chemical reagents	
IPTG	Anatrace®
PBS	Sigma Aldrich®
NaOH	Fisher Scientific®
NaCl	Sigma Aldrich®
Glycerol	Fisher Scientific®
Sodium phosphate, dibasic dodecahydrate	Honeywell®
Sodium phosphate, monobasic dihydrate	Fisher Scientific®
Imidazole	Sigma Aldrich®
DDM	Anatrace® or Glycon®
TCEP-HCl	Thermo Scientific®
MTSSL	Santa Cruz or Toronto Research Chemicals
Ampicillin	Formedium®
LB Agar, Miller	Sigma Aldrich®
LB Media, Miller	Sigma Aldrich®
Deuterated ethylene glycol	Sigma Aldrich®
Software	
SnapGene® by Dotmatics	https://www.snapgene.com/
Pymol	https://pymol.org/ [61]
VMD	https://www.ks.uiuc.edu/Research/vmd/ [62]
CHARMM GUI	https://www.charmm-gui.org/ [63]
GROMACS 2016.4	https://www.gromacs.org/ [64]
OriginPro®2022b	OriginLab Corporation, Northampton, MA, USA https://www.originlab.com/
Recombinant DNA	
Plasmid: pTrc cys-free MscM	Dr Andrew Hartley
Bacterial strains	

<i>E. coli</i> DH5 Alpha cells	Thermo Fisher Scientific®
<i>E. coli</i> MJF641 cells	Thermo Fisher Scientific®
Other	
Ni-NTA agarose resin	Invitrogen®
BioBeads SM-2 adsorbents	Bio-Rad®

2.1.2 Buffers composition

Protein purification buffers	
PBS buffer	8g NaCl, 0.2g KCl, 1.15g Na ₂ HPO ₄ ·7H ₂ O and 0.2g KH ₂ PO ₄ per liter
Solubilisation buffer	50 mM NaPO ₄ , 300 mM NaCl, 10% Glycerol, 25 mM imidazole, 0.1 mM PMSF, 1% DDM, pH 7.5
Wash buffer	50 mM NaPO ₄ , 300 mM NaCl, 25 mM imidazole, 0.1 mM PMSF, 0.05% DDM, pH 7.5
Elution buffer 1	50 mM NaPO ₄ , 300 mM NaCl, <u>150 mM imidazole</u> , 0.05% DDM, pH 7.5
TCEP buffer	50 mM NaPO ₄ , 300 mM NaCl, 25 mM imidazole, 5 mM TCEP, 0.05% DDM, pH 7.5
MTSSL buffer	50 mM NaPO ₄ , 300 mM NaCl, 25 mM imidazole, 1 mM MTSSL, 0.05% DDM, pH 7.5
Elution buffer 2	50 mM NaPO ₄ , 300 mM NaCl, 300 mM imidazole, 0.05% DDM, pH 7.5
Size exclusion chromatography (SEC) buffer	50 mM NaPO ₄ , 300 mM NaCl, 0.05% DDM, pH 7.5
Lipid bilayer reconstitution buffers	

Lipid solubilisation buffer	50 mM NaPO ₄ , 300 mM NaCl, 1% DDM, pH 7.5
Reconstitution buffer	50 mM NaPO ₄ , 300 mM NaCl, pH 7.5

2.1.3 Oligonucleotides

The primers of mutants designed for this thesis. The primers for mutants V553C, R737C, R631C and L519C were designed by Dr Andrew Hartley, Piotas Lab.

Primer: MscM D618C Forward GATGATGTTCTGTAACCTCGACGACCGTGAATTCTCCGGTTCGCTGGGAC
Primer: MscM D618C Reverse CGAGGTTACAGAACATCATCAGCGCCATAATCAGCGGCACAATAAGCCCG
Primer: MscM K464C Forward GTTGGGCTGTGCCAGTGTGATGATGCTGACCAGCAAAGAGACAATTTTGC
Primer: MscM K464C Reverse CACTGGCACAGCCCAACTGACTGAAGGTGTCCAGCGAAATGAGACGACGC
Primer: MscM L477C Forward GAGACAATTTGTCCGCTGTTTGGCGCGTTGATTCTGGTCGGTTGCAGTATTTAC
Primer: MscM L477C Reverse CAGCGGACAAATTGTCTCTTTGCTGGTCAGCATCATCACACTGGCTTTGC

2.2 Methods

Biochemistry

2.2.1 PCR

Site-directed mutagenesis reactions were completed using primers to introduce point mutations. Cysteine mutants of MscM were designed using the SnapGene protocol. Mutant R631C was designed by Dr Andrew Hartley. PCR was done using the NEB PCR kit, contents of the kit include 5x Q5 Reaction Buffer, dNTPs, Q5 High-Fidelity DNA Polymerase. A stock of 100 μ M primers were made and a working stock of 10 μ M primers were made. Reaction components were assembled in a PCR tube in the order starting with PCR water and the final component added was Q5 High-Fidelity DNA polymerase. The PCR reaction mixture consisted of 0.25 μ L of Q5 DNA polymerase, 2.5 μ L of 2mM dNTPs, 5 μ L of 5x Q5 reaction buffer, 1.25 μ L of 10 μ M forward primer, 1.25 μ L of 10 μ M reverse primer, and PCR water to make up the volume to 25 μ L. PCR tubes were transferred to a PCR machine for thermocycling (Table 1).

Step	Temperature	Time
Initial Denaturation	98°C	30s
25-35 Cycles:		
Denaturation	98°C	20s
Annealing	60°C	20s
Extension	72°C	4 minutes
Final Extension	72°C	8 minutes
Hold	4°C	

Table 1: PCR conditions for thermocycling.

2.2.2 Transformation to bacterial cells for genotype sequencing

1 μ L of Dpn1 was added to 10 μ L of PCR product and incubated at 37°C for 2 hours.

Eppendorf tubes of *E. coli* DH5 α cells were retrieved from -80°C and thawed on ice.

10 μ L of Dpn1 incubated PCR product was added to 100 μ L of DH5 α cells and gently mixed and incubated on ice for 30 minutes. The incubated mixture was heat shocked at 42°C for 60 seconds and then returned to ice for 2 minutes. Subsequently, 1 mL room temperature Luria

Broth (LB) media was added and left in a shaking incubator at 37°C for 1 hour. 100 mg/mL Ampicillin using 1:1000 dilution was used to prepare LB Agar plates. The transformation was centrifuged at 6000RPM for 1 minute and most of the supernatant was discarded. 100 µL of the transformation was resuspended and spread on the Ampicillin LB Agar plates. The plates were incubated at 37°C overnight. The following morning the plates were examined for bacterial colonies and stored at 4°C.

2.2.3 Overnight cultures

Bacterial colonies were picked from an appropriate Ampicillin LB Agar plate or was scraped off a glycerol stock stored at -80°C using inoculating loops and transferred into 20 mL aliquots of LB Miller liquid media. The number of aliquots were based on the volume of cell culture, a ratio of 1:100 overnight culture: cell culture was used. The starter cultures were labelled and left to incubate overnight in a rotating incubator at 37°C, shaking at 200 RPM.

2.2.4 Miniprep

Overnight cultures of 5 mL aliquots were prepared, and plasmids were extracted using the Qiagen miniprep kit. The protocol of the kit was followed exactly, although the wash with Buffer PE was done twice and subsequently, a 2-minute spin was done and left to stand for 10 minutes to allow residual ethanol to evaporate. The final elution was done using 50 µL of H₂O.

2.2.5 Plasmid Sequencing

The concentration of extracted plasmids was measured and samples between 50-100 ng/µL were prepared using appropriate primers and sent out for sequencing to Genewiz, Azenta Life Sciences.

2.2.6 Plasmid transformation

1 µL of plasmid was gently mixed into 100 µL of MJF641 cells and incubated on ice for 30 minutes. The incubated mixture was heat shocked at 42°C for 60 seconds and then returned to ice for 2 minutes. Subsequently, 1 mL room temperature LB media was added and left in a shaking incubator at 37°C for 1 hour. LB agar plates with 1:1000 dilution Ampicillin were

prepared. 100 μ L of the transformed cells were spread on the Ampicillin plate and incubated at 37°C overnight. The plates were stored in 4°C refrigerators the following morning.

2.2.7 Cell culture and protein purification

2.2.7.1 Cell growth

5 mL of overnight culture were transferred into 500 mL of autoclaved LB media the following morning. The LB media were incubated at 37°C at 200 RPM. The cells were grown until OD at 600 nm reached ~0.8-1.0 (late-exponential phase). The culture was cooled to 25°C and final concentration of 1 mM IPTG (isopropyl-beta-D-thiogalactoside) was added to induce protein expression for a further 3.5-4.5 hours. Cells were harvested by centrifugation at 5000 RPM for 10 minutes. The supernatant was discarded, and the pellets were retained. Cell pellets were weighed and resuspended in 20 mL aliquots of ice-cold PBS buffer (8g NaCl, 0.2g KCl, 1.15g Na₂HPO₄·7H₂O and 0.2g KH₂PO₄ per liter). The cell pellets were frozen and stored at -80°C until required.

2.2.7.2 MscM protein purification

The column used for affinity chromatography was of 1 mL and the corresponding volumes of column washes of buffers used has been described in the protocol described below. The membrane protein purification was completed as previously described [12] [65].

Cell pellets were taken out of -80°C and homogenised with 10 mL of ice-cold PBS buffer for every 1g of cells. The cells were lysed using a cell disruptor at 30kpsi. The cells were centrifuged at 5000 RPM for 30 minutes to remove cell debris. The supernatant was centrifuged at 40,000 RPM at 4°C for 1 hour to harvest cell membrane pellets. The membrane pellets were weighed to determine the volume of solubilisation buffer (50 mM NaPO₄, 300 mM NaCl, 10% Glycerol, 25mM imidazole, 0.1 mM PMSF, 1% DDM, pH 7.5) required. 25 mL of solubilisation buffer was used for every 1g of membrane pellet.

Membranes were solubilised on ice using a precooled 55 mL Dounce homogeniser and left to incubate at 4°C for 1 hour on a rotating wheel. The solubilised membranes were centrifuged at 30,000 RPM at 4°C for 30 minutes to remove insoluble material. A HisTrap HP column containing 1 mL of nickel-nitrilotriacetic acid (Ni²⁺-NTA) agarose was equilibrated at 4°C using the solubilisation buffer and the solubilised proteins were loaded at a flow rate of

~0.6-0.75 mL/min. After all the solubilised material was allowed to pass through, 5 mL of wash buffer (50 mM NaPO₄, 300 mM NaCl, 25 mM imidazole, 0.1 mM PMSF, 0.05% DDM, pH 7.5) was used to wash the resin. The contaminant, cytochrome bo₃, was eluted using 10 mL of elution buffer 1 (50 mM NaPO₄, 300 mM NaCl, 150 mM imidazole, 0.05% DDM, pH 7.5). The resin was washed with 5 mL of TCEP buffer (50 mM NaPO₄, 300 mM NaCl, 25 mM imidazole, 5 mM TCEP, 0.05% DDM, pH 7.5) and left to equilibrate for 30 minutes. The resin was washed with 3 mL of wash buffer and then washed with 3-5 mL MTSSL buffer (50 mM NaPO₄, 300 mM NaCl, 25 mM imidazole, 1 mM MTSSL, 0.05% DDM, pH 7.5). The resin was left to equilibrate for 1 hour. The resin was further washed with 2-5 mL of MTSSL buffer and left for an additional hour or overnight. The resin was washed with 10 mL of wash buffer to remove unbound MTSSL. Bound MscM was eluted using 18 mL of elution buffer 2 (50 mM NaPO₄, 300 mM NaCl, 300 mM imidazole, 0.05% DDM, pH 7.5). Concentration of the elution was measured using a nanodrop. The elution fraction was concentrated using 100 kDa MWCO Vivaspin centrifugal concentrators at 2800 RPM at intervals of 7 minutes at 4°C. After every 7 minutes, the samples were resuspended by pipetting to avoid aggregation of protein. The volume was brought down to ~0.8-1.0 mL and concentration of the samples were recorded. Concentrated protein samples were spun at 13,000 RPM for 10 minutes before size exclusion chromatography (SEC). The supernatant was loaded using a 1 mL Hamilton syringe onto a 120-mL Superose 6 column that was previously equilibrated with degassed, cold SEC buffer (50 mM NaPO₄, 300 mM NaCl, 0.05% DDM, pH 7.5). Labelled protein was eluted at 0.20 mL/min and absorption at 280 nm was recorded. 0.2 mL fractions were collected in a 96-well plate. The fractions of the MscM heptamer peak were pooled and concentrated using a 100 kDa MWCO Vivaspin centrifugal concentrator until the protein concentration was higher than ~3.5 mg/mL.

2.2.7.3 cwEPR measurements

cwEPR measurements of the samples were recorded at 4°C using Bruker Magnettech ESR5000 X-band spectrometer to measure the spin labelling efficiency of the protein sample. The protocol previously proposed [66] [65] was used to complete cwEPR measurements. A Hamilton syringe attached to a thin plastic capillary tube was used to load 40 µL of spin-labelled protein sample into a bottom sealed glass EPR tube. The Bruker

Magnettech ESR5000 X-band cwEPR spectrometer was switched on and the Warm-up recipe was selected on the ESRStudio software and initialised. A routine warm-up of 15 minutes was completed and the BioTemperature controller connected to a nitrogen gas supply was switched on. The measuring recipe was selected, and the temperature of the spectrometer was brought down to 4°C, the cool-down process takes ~30 minutes. Once the temperature was stabilised at 4°C, the EPR tube was positioned accurately into the holder of the spectrometer. The measurements were recorded and samples with signal intensity greater than 25 were prepared for PELDOR spectroscopy. For PELDOR spectroscopy, samples were transferred from the EPR tube into a labelled Eppendorf tube and 25 µL of deuterated ethylene glycol was added to 40 µL of spin-labelled protein samples and mixed carefully. Deuterated ethylene glycol was added as a cryoprotective agent. The Eppendorf tubes were snap frozen in liquid nitrogen and stored at -80°C.

2.2.7.4 Imidazole gradient optimisation

The protein purification protocol adopted by Dr Andrew Hartley, Pliotas Lab was used to purify MscM. On observation of MscM monomer band on elution 1 of a protein purification gel, an imidazole optimisation of elution buffer 1 was employed to optimise the protein purification. The optimisation was carried out twice using ÄKTA where the prepacked HisTrap (HP) column used for the purification was connected. Imidazole optimisation was performed using 25 mM imidazole wash buffer (Buffer A) and 150 mM imidazole elution buffer 1 (Buffer B). The percentage of Buffer B was increased as a gradient, remainder volume of buffer was made up by Buffer A. The percentage of Buffer B was increased until elution of the contaminant- cytochrome bo_3 was seen at 280 nm. The final concentration of imidazole was calculated by a summative value of imidazole concentrations of Buffers A & B. The concentration of Buffer B was increased until 15% and eluant was collected as 200 µl fractions, as percentage of Buffer B was increased. The column was disconnected, and purification steps were resumed as given in Section 2.2.7.2. The revised imidazole concentration of 45mM was used for elution 1 buffers for the following purifications. The optimised elution 1 buffer composition was 50 mM $NaPO_4$, 300 mM NaCl, 45 mM imidazole, 0.05% DDM, pH 7.5.

2.2.8 Preparing lipids for reconstitution experiments

SoyPC lipids were used for all the reconstitution experiments in this project. The appropriate volume of SoyPC lipid stock was stored as 10 mg/mL in chloroform at -20°C and transferred to a glass bottle. Chloroform was evaporated using nitrogen gas in a fumigation cupboard. Once a thin film of lipids was seen on the bottle, a volume of lipid solubilisation buffer (50 mM NaPO₄, 300 mM NaCl, 1% DDM) was added to resuspend the lipids at the desired concentration of SoyPC. To homogenise the lipids in the solubilisation buffer, the lipids were sonicated in a sonicating water bath for ~10 minutes and then placed on a rotating wheel for ~10 minutes. This was repeated until the lipids were homogenised and the resulting solution was clear.

2.2.9 SapA nanodisc reconstitution

The protocol proposed by Flayhan et. al. [67], was adopted for reconstitution of MscM in SapA nanodiscs. SapA nanodiscs were made using concentrated MscM, SoyPC lipids and purified SapA. SapA was purified by Bolin Wang, Pliotas Lab. MscM was purified using the protein purification protocol in Section 2.2.7.2. Lipids were prepared for reconstitution as described in Section 2.2.8. A₂₈₀ of the purified SapA stock was measured. The volume of SapA to be used was calculated using the ratio of MscM:SoyPC:SapA required.

Volume of SoyPC required depending on the ratio of MscM:SoyPC:SapA was added to the appropriate volume of SapA and MscM. The MscM/SoyPC/SapA mixture was incubated for 30 minutes on ice. Damp BioBeads SM-2 adsorbents were weighed out by calculating 50x the concentration of DDM in the incubated mixture. BioBeads were washed two times with water and two times with a reconstitution buffer (50 mM NaPO₄, 300mM NaCl). The BioBeads were added in three instalments, after each addition of BioBeads, the MscM/SoyPC/SapA mixture was incubated for 30 minutes on a rotating wheel at 4°C. After the final addition of BioBeads, the mixture was left to incubate overnight (~16 hours). The next day morning, the mixture was extracted using a Hamilton syringe and transferred into a pre-cooled Eppendorf tube. Based on the volume of the mixture, the volume was brought down to ~0.8-1.0 mL by concentrating at 1500g at 5-minute intervals. Concentrated samples were spun at 13,000RPM for 10 minutes before size exclusion chromatography. The

supernatant was loaded using a 1 mL Hamilton syringe onto a 120-mL Superose 6 column (Cytiva) equilibrated with degassed, cold reconstitution buffer. The appropriate peak of SapA:MscM was collected and concentrated down until a concentration higher than ~3.5 mg/mL was achieved.

2.2.10 SapA nanodisc reconstitution optimisation

Optimisation of SapA nanodisc reconstitution was employed to increase the yield of reconstituted MscM. The protocol proposed by Flayhan et. al., was adopted to test the best ratio for highest yield. Four ratios of MscM:SapA:SoyPC were tested-

1:15:35, 1:15:70, 1:20:35, 1:20:70. The optimisation was completed with smaller reconstitution batches with 10 μ L of purified MscM and appropriate volumes of SapA and SoyPC according to the ratios. Since the reconstitution volumes were <50 μ L, a Superose 6 5/150 column was used. The resultant size exclusion chromatography profiles were assessed to identify the optimized ratio for reconstitution.

2.2.11 Liposome reconstitution

SoyPC for liposome reconstitution was prepared using the protocol explained in Section 2.2.8. The volume of SoyPC required depending on the ratio of MscM:SoyPC liposome was added to the appropriate volume of purified MscM. The ratio of MscM:SoyPC used for the liposome reconstitution experiments was 1:10. The MscM/SoyPC mixture was incubated for 30 minutes on ice. Damp BioBeads 50x the DDM concentration in the MscM/SoyPC mixture was weighed out and washed two times with water and two times with a reconstitution buffer (50 mM NaPO₄, 300 mM NaCl). After each addition of BioBeads, the MscM/SoyPC mixture was incubated for 30 minutes on a rotating wheel at 4°C. After the final addition of BioBeads, the mixture was left to incubate overnight. The next day morning, the mixture was extracted using a Hamilton syringe and transferred into a pre-cooled Eppendorf tube. The sample was topped up to 5 mL with reconstitution buffer and centrifuged at 40,000 RPM at 4°C for 1 hour. The supernatant was discarded, and the pellet was resuspended in 40 μ L reconstitution buffer. The concentration was recorded and cwEPR measurements were recorded using the protocol described in Section 2.2.7.3.

2.2.12 Molecular Dynamics simulations

The MD simulations were set up using CHARMM-GUI. The MscS structure (PDB:6RLD) in the closed state was inserted in a symmetric bilayer containing 184 DOPC lipids, occupying an area of 187 x 187 Å. System was neutralised with 150 mM concentration of NaCl. Following the equilibration of CHARMM-GUI [63], the system was energy minimised and equilibrated in six steps. The systems were simulated using GROMACS_2016.4 [64] in an NPT ensemble at 303.15K with CHARMM36 force field and 2 fs time step. The production scripts generated by CHARMM-GUI were optimised with the help of Bolin Wang, Pliotas Lab. The analysis of the simulation was completed using GROMACS commands – gmx pairdist to calculate the distance between protein residue 67 and desired region of DOPC acyl chains, gmx select to calculate the number of the acyl chains present within 15Å of protein residue 67 and to calculate the number of acyl chains present within 5Å of pocket residue. VMD [62] and PyMol [61] were used to visually analyse and validate GROMACS commands data. OriginPro®2022b was used for graphical representation of data.

Chapter 3: Results and Discussion - Experimental and computational investigation of MscS-like channels

MscM – MS channel of mini conductance is a bacterial MS channel of the MscS-like family, with a reported conductance of $\sim 0.30\text{nS}$ [9]. MscM is known to be a homoheptamer of $\sim 900\text{kDa}$ with an unresolved structure [10]. Previous studies have shown that conformational states of MS channels in detergent occasionally change when reconstituted into lipids [68]. Mechanical sensing for some membrane protein channels has been shown to be dependent on nanopockets (NP) within proteins [2], and delipidation of these pockets is known to be necessary for the activation of MS channels [69].

This chapter covers the sample preparation of MscM mutants for the structural characterisation of MscM using PELDOR spectroscopy. The project aims to feed experimental data from PELDOR into MD simulations. The interaction of lipids and proteins are observed using experimental and computational methods. Eventually, from the cocktail curated of experimental and computational techniques, the project aims to assemble a structure of MscM and its dynamic transition landscape. The experimental aspect of this thesis is mainly focused on preparation of MscM samples in two conditions – in detergent (DDM) and in native lipid environment. It was hypothesised that PELDOR data would differ between MscM in DDM and MscM in native lipid environment. Purification of membrane proteins is based on the principle of immobilized metal affinity chromatography (IMAC). Recombinant His-tagged proteins bind to Ni^{2+} -nitrilotriacetic acid (Ni – NTA) resin beads, this technique separates target membrane proteins from other proteins. During the project, purification protocol steps were optimised to increase efficiency and yield of purification. This chapter also includes the results of reconstitution experiments of MscM within different native lipid environment systems to identify the ideal system for PELDOR sample preparation. For high-sensitivity data gathering using PELDOR, high spin-labelling efficiency is necessary. Hence, signal intensity of spin labels is a determining factor during sample preparation for PELDOR [41]. This was measured by cwEPR, prior to acquiring PELDOR data. MscM heptamer was assembled using AlphaFold software by Dr Andrew Hartley, Pliotas Lab. The AlphaFold models provided the foundation of the MscM monomer to assemble the heptamer, single-cysteine mutants on

transmembrane helices were modified as described in Methods Section 2.2.1 (Fig. 1). The computational work of this thesis consisted of an MD simulation of the well-studied structure, MscS in an MSP1E3D1 nanodisc – native lipid environment, over a long timescale to investigate protein-lipid dynamics.

3.1 Dynamics of MscM gating by PELDOR and AlphaFold

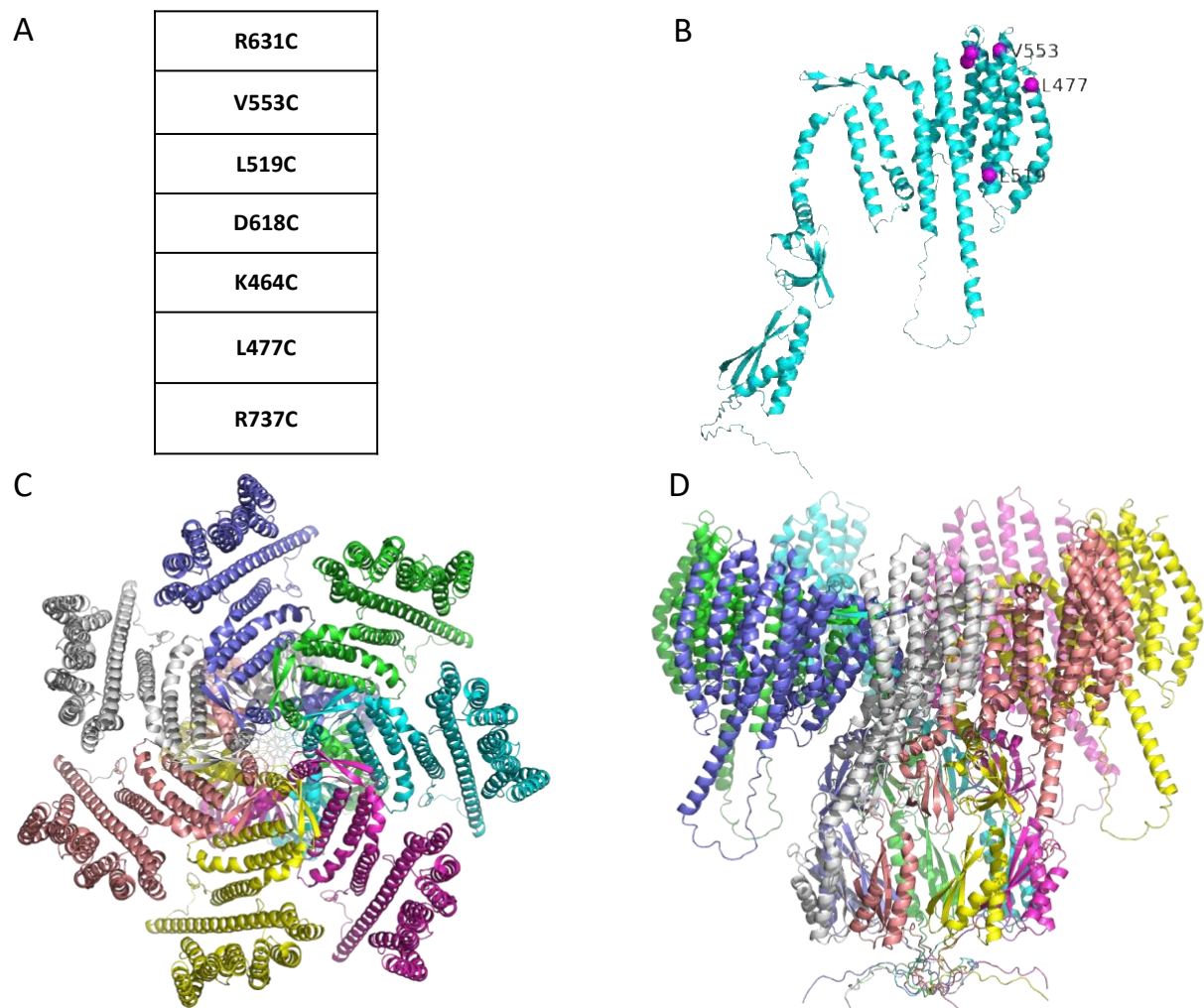


Figure 1: Mutants of MscM prepared in the scope of this thesis.

Mutants purified as part of this (A). Snapshots of AlphaFold models of MscM assembled by Dr Andrew Hartley, Pliotas Lab using PyMol [61] (B, C, D): A monomer of MscM, cysteine mutants purified have been labelled (magenta spheres) *. MscM heptamer from the top view (C) and side view, permeation pathway from periplasm to the

cytoplasm is seen (D). Each subunit is represented by a different colour. *K464C has not been labelled in the monomer in (B) as the sequence of the MscM AlphaFold model is truncated from the N-terminus.

3.1.1 MscM purification

The purification and yield were optimised by comparing binding efficiencies of two types of Ni²⁺-nitrilotriacetic acid (Ni – NTA) resin columns – gravity glass column and prepacked HisTrap High Performance (HP) column. The purification of L519C mutant using the two columns showed the yield of the protein purification was higher using the prepacked column (Fig. 2A).

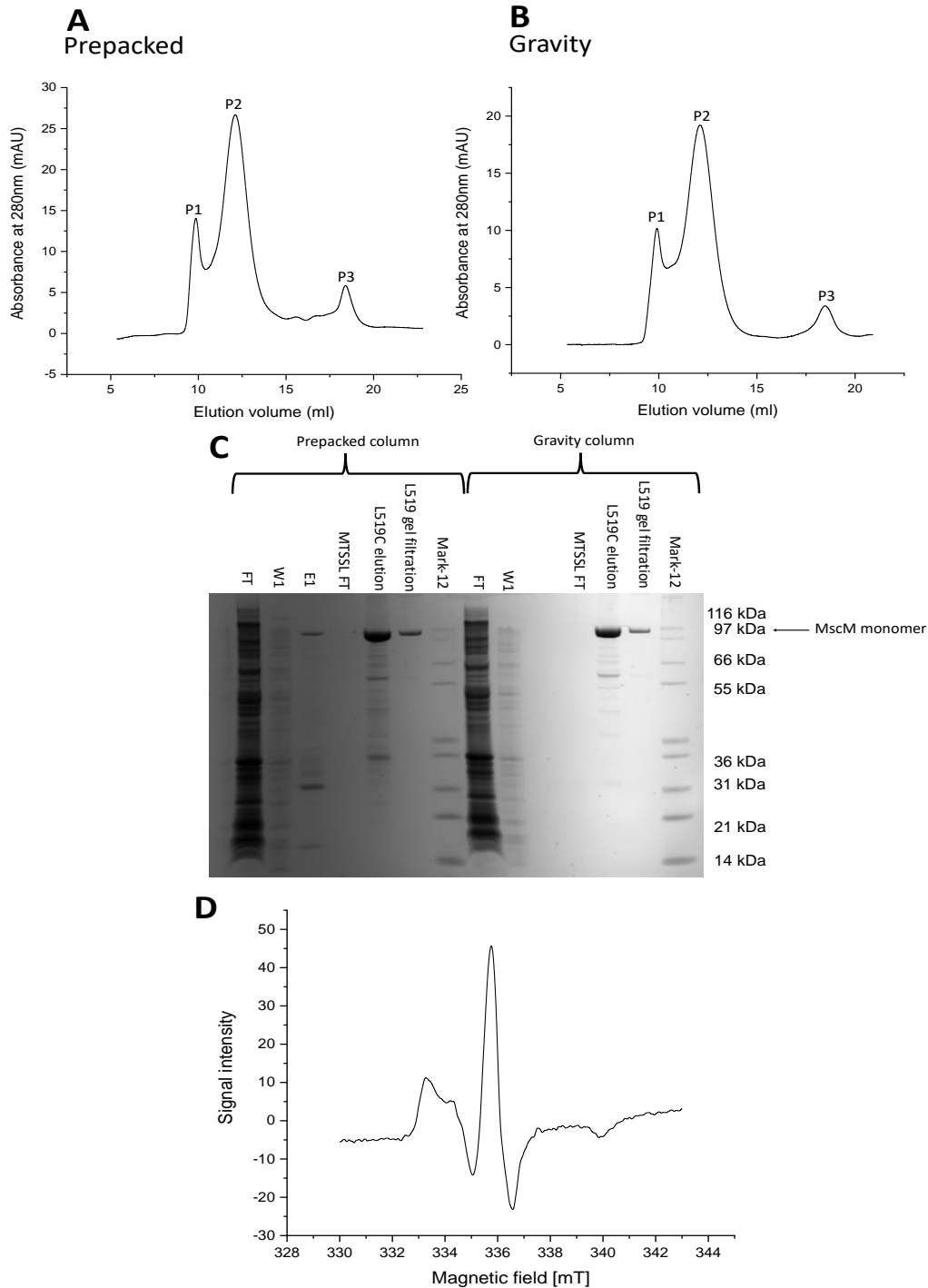


Figure 2: Protein purification of L519R1.

Comparison of gel filtration profiles using prepacked column (A) and gravity glass column (B), P1- MscM aggregation, P2 – MscM heptamer, P3 – dissociation product.

SDS-PAGE gel of protein purification samples from both columns (C). FT – solubilised membrane flow through, W1 – Wash buffer 1, E1 – Elution 1, MTSSL FT – MTSSL flow through, L519R1 elution – Elution 2, L519R1 gel filtration – protein sample after size exclusion

chromatography, Mark-12 – protein ladder. The cwEPR spectrum of MscM L519R1 in DDM (D).

The results showed the binding efficiency of the prepacked HisTrap HP column was higher than the glass gravity column. The resin, which is composed of highly cross-linked agarose beads to which a chelating group is attached, is most likely to be the reason for the high performance of the prepacked HisTrap HP column. Tetradentate chelating ligands such as, Ni^{2+} -nitrilotriacetic acid matrices have two exposed transition metal coordination sites where affinity tags of proteins can interact [70]. Proteins with exposed histidine groups, such as our recombinant His-tagged proteins, are selectively retained by the nickel-precharged chelating groups (Bio-Rad®). The resin can be exposed to various conditions like detergents and protein denaturants. Additionally, the stability of transition metal ion binding allows regeneration of the resin, making the columns reusable [70].

The following purifications were completed using the prepacked HisTrap HP column.

3.1.2 Imidazole gradient optimisation

The purity of MscM was examined during each step of the sample preparation. Following the identification of the best column for purification, the wash steps were observed to identify room for optimisation. Elution 1 of the prepacked column showed a weak band at 97kDa corresponding to MscM monomer (Fig. 2C). To reduce the loss of protein during elution 1, an imidazole optimisation of elution 1 buffer was employed using the conditions described in Methods Section 2.2.7.4. Elution buffer 1 gradient when increased to 15% was seen to elute protein at 280nm, and elution of protein was seen to decrease when the buffer percentage was maintained at plateau. Further increase of elution buffer 1 up to 25%, was seen to elute more protein, the corresponding eluant was run on an SDS-PAGE gel (lane E1.9 of gel R631C (Fig. 3C)) and shows a weak band at MscM monomer. The imidazole optimisation showed 25 mL 45mM elution buffer 1 was sufficient to elute contaminant cytochrome bo_3 . The gel filtration profiles, and SDS-PAGE gels of the mutants used for imidazole optimisation (V553C and R631C) show the intensity of the band of MscM monomer increase with increasing percentage of elution 1 buffer (Fig. 3C, lanes E1.7, E1.8, E1.9). Following purification

employed the optimised imidazole concentration, MscM monomer band was not as distinctly visible in the elution 1 SDS-PAGE gel lanes (Fig. 4C).

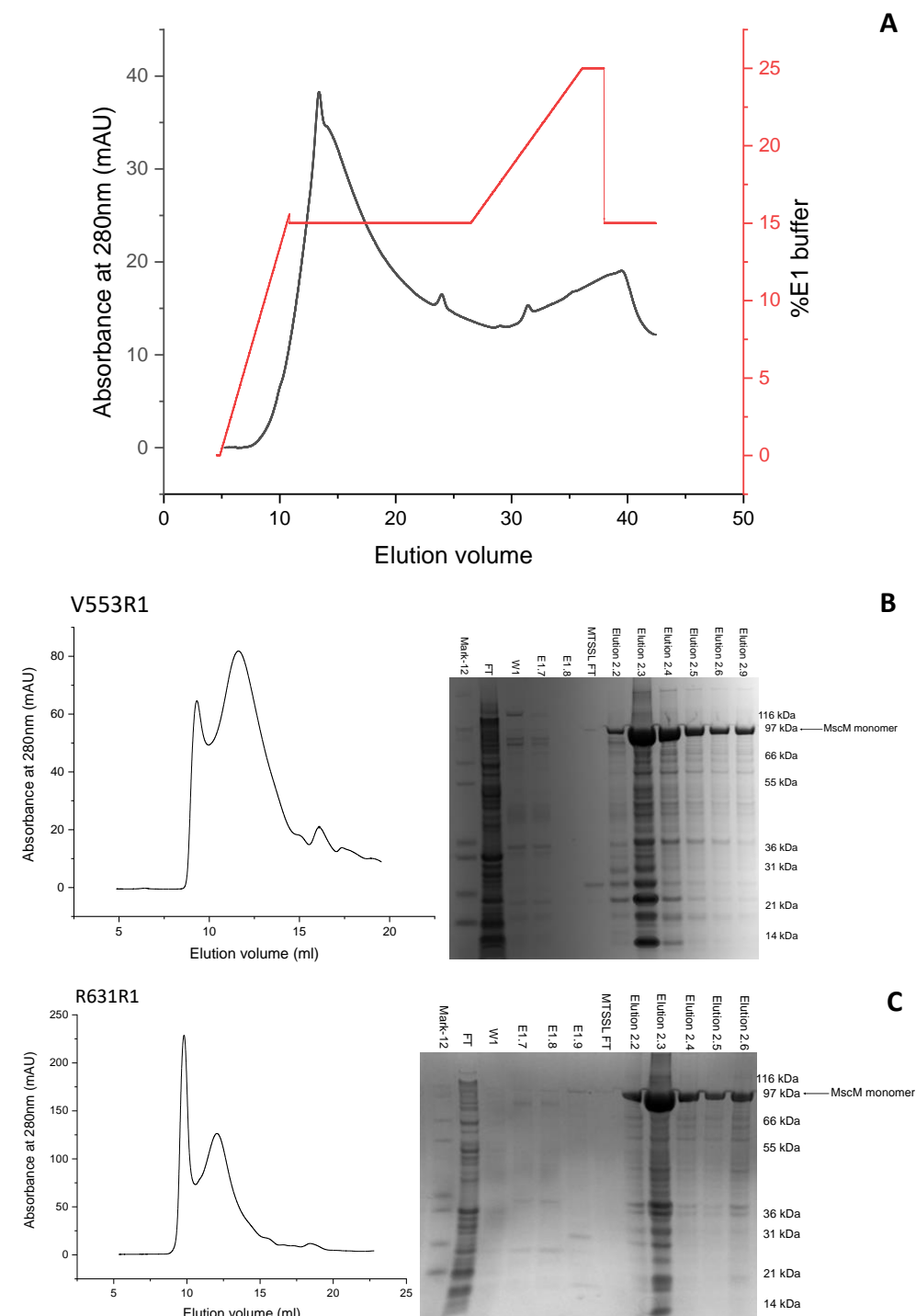


Figure 3: Imidazole optimisation of elution 1 using ÄKTA Pure. Red slope represents the gradient of Buffer A passed through the column. Dark grey represents elution at 280nm. Gel filtration profiles and SDS-PAGE gels of the mutants used for imidazole optimisation (B, C).

One of the disadvantages of IMAC is nonspecific binding of proteins with exposed histidine residues. Coelution of these untagged proteins results in contamination, therefore affecting the purity of the purification products. Nonspecific binding of proteins to the column can be reduced by two methods: Imidazole in the elution buffer 1 or reducing the pH of the wash buffer to lower than the pH of the wash buffer. The protocol we adopted used imidazole for more stringent wash and elution steps. The use of imidazole is preferred over low pH exposure as this may affect the tertiary structure of our protein of interest [70]. Imidazole elutes the bound protein by a competitive mechanism. It has a structure that is similar to that of histidine and competes with the protein of interest to bind to the Ni^{2+} -nitrilotriacetic acid matrices, and therefore elutes the bound protein [70].

3.1.3 MscM in detergent

The purification of MscM in DDM produced a high yield with all the mutants (Fig. 4). The final concentration of DDM samples for PELDOR were greater than 4 mg/mL. Mutant proteins with the MTSSL bound to the mutated cysteine are represented as V553R1 or L737R1 etc. The cwEPR spectra of the DDM samples were of high quality and displayed good spin-labelling efficiency. All DDM samples produced high cwEPR signals greater than 55. The spin-labelling efficiency of the samples were suitable to proceed for PELDOR. The cwEPR spectra of the mutants in DDM show intermediate to slow mobility. The broad spectrum of the spectra represents restricted spin label motion [12] [71]. Mutants L477R1 and L737R1 revealed higher mobility than the other mutants (Fig. 6D & 7). L477R1 had the highest mobility and D618R1 showed the least (Fig. 6D & 6B). With the cwEPR spectra, the environmental conditions of the spin label can be assessed, giving an insight into the dynamics of the different transmembrane helices.

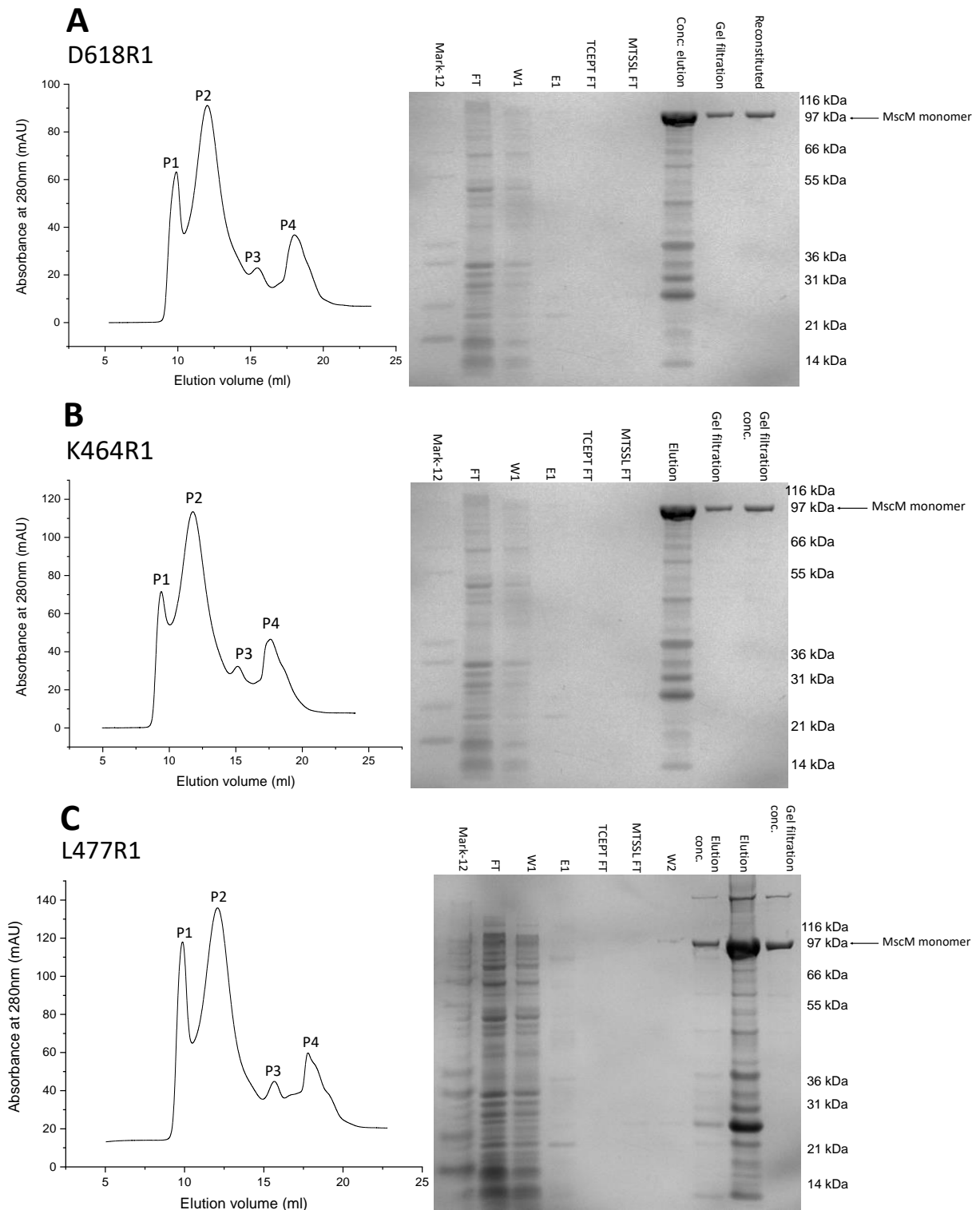


Figure 4: Protein purification of MscM mutants.

Gel filtration profiles (left) and SDS-PAGE gels (right) of MscM purification samples. Gel filtration profiles: P1- MscM aggregation, P2- MscM heptamer, P3 & P4- dissociation products. SDS-PAGE gels: Mark-12-protein ladder, FT-solubilised membrane flow through, W1-wash 1, E1-elution 1, TCEP FT-TCEP flow through, MTSSL FT-MTSSL flow through, W2-

wash 2, Elution-elution 2, Elution conc. - concentrated sample of elution 2, Gel filtration-P2 of gel filtration, Gel filtration conc.-concentrated sample of P2, Reconstituted-MscM reconstituted in SoyPC liposome. The higher band above MscM monomer was confirmed to be a MscM oligomer by mass spectrometry completed by Bolin Wang, Piotas Lab (Fig. 4C).

3.1.4 Reconstitution of MscM in lipid environments

On completion of the DDM samples preparation, the next phase of the experimental aspect of the project was attempted. Mutants on the external helices of MscM monomer – V553C, K464C, L477C, D618C (Fig. 1) and one mutant on the long transmembrane helix of MscM, R737C, were selected to attempt reconstitution within native lipid environment systems. The long transmembrane helix of MscM is hypothesised to be unique to MscM.

Ward et al., reconstituted MscS in two types of lipid bilayer systems: nanodiscs and bicelles, to observe the protein within lipid bilayer systems using PELDOR [72]. They reported that MscS could adopt both closed and open states within lipid bilayers, this was previously seen in detergent solution as well. The PELDOR data from lipid reconstituted protein showed a difference in modulations and oscillations when compared to samples in detergent. More damped oscillations and shallower modulations were seen in the lipid samples. Broad distance distributions are formed from damped oscillations, this could suggest the conformational flexibility of MscS is increased in lipid systems [72].

3.1.5 SapA nanodisc reconstitution

Reconstitution was attempted in SapA nanodiscs and liposomes. Reconstitution was attempted in SapA nanodiscs initially using the MscM:SapA:SoyPC in a molar ratio of 1:15:35, but this has failed multiple times. Fig. 5B shows a representative gel filtration profile of MscM-SapA reconstitution experiments using the molar ratio of 1:15:35. Aggregation was a significant limiting factor in the experiments (indicated by * on Fig. 5B). The aggregation peak was approximately seven times the yield of reconstituted MscM.

To optimise the experiment, a small-scale SapA reconstitution screening was employed using different stoichiometric ratios, following the protocol proposed by Flayhan et. al [67]. All the four conditions of reconstitution gave a high peak of free SapA molecules (indicated by ^ in

Fig. 5A). The protein aggregate peak eluted was almost indistinguishable with the MscM reconstituted peak for molar ratios 1:15:35 and 1:15:70. The molar ratios 1:20:35 and 1:20:70, eluted individual homogenous peaks of the soluble protein aggregates, reconstituted protein and free SapA molecules. The two ratios produced a similar elution profile, the MscM:SapA:SoyPC ratio of 1:20:70 was adopted as it gave a higher yield compared to 1:20:35. Following optimization, the reconstitution experiments were repeated using the optimised molar ratio of 1:20:70, the gel filtration profile of the reconstitution experiment was different, peaks of soluble aggregates and free SapA molecules were seen. The gel filtration profile resulted in a homogenous reconstituted MscM peak, which was approximately three times higher than prior to optimization. The resultant volumes of MscM reconstitution in SapA nanodiscs, after size exclusion chromatography and concentration, were less than 4 μ L with less than 3 mg/mL protein concentration. The sample volumes were insufficient for cwEPR and PELDOR measurements, despite an increase in yield after the optimisation experiments. This resulted in opting another native lipid environment system for reconstitution.

Studies have shown that an excess of lipids with insufficient amounts of SapA hinders the process of reconstitution [67]. They hypothesised that excess free lipid molecules in solution shifts the equilibrium to form empty nanoparticles, causing aggregation of membrane protein due to a deficit of SapA supply required for proper reconstitution. The study suggests an adequate amount of lipid molecules and a surplus of Saposin to allow proper reconstitution and avoid aggregation of the membrane protein [67]. This supports the optimisation results, the best ratios (1:20:70 and 1:20:35, Fig. 5A) had the highest molar ratios of SapA. Despite using the higher ratio of SapA, the reconstitution gel filtration profile showed a high peak of free SapA molecules (Fig. 5C), suggesting room for further screening of the stoichiometric ratios.

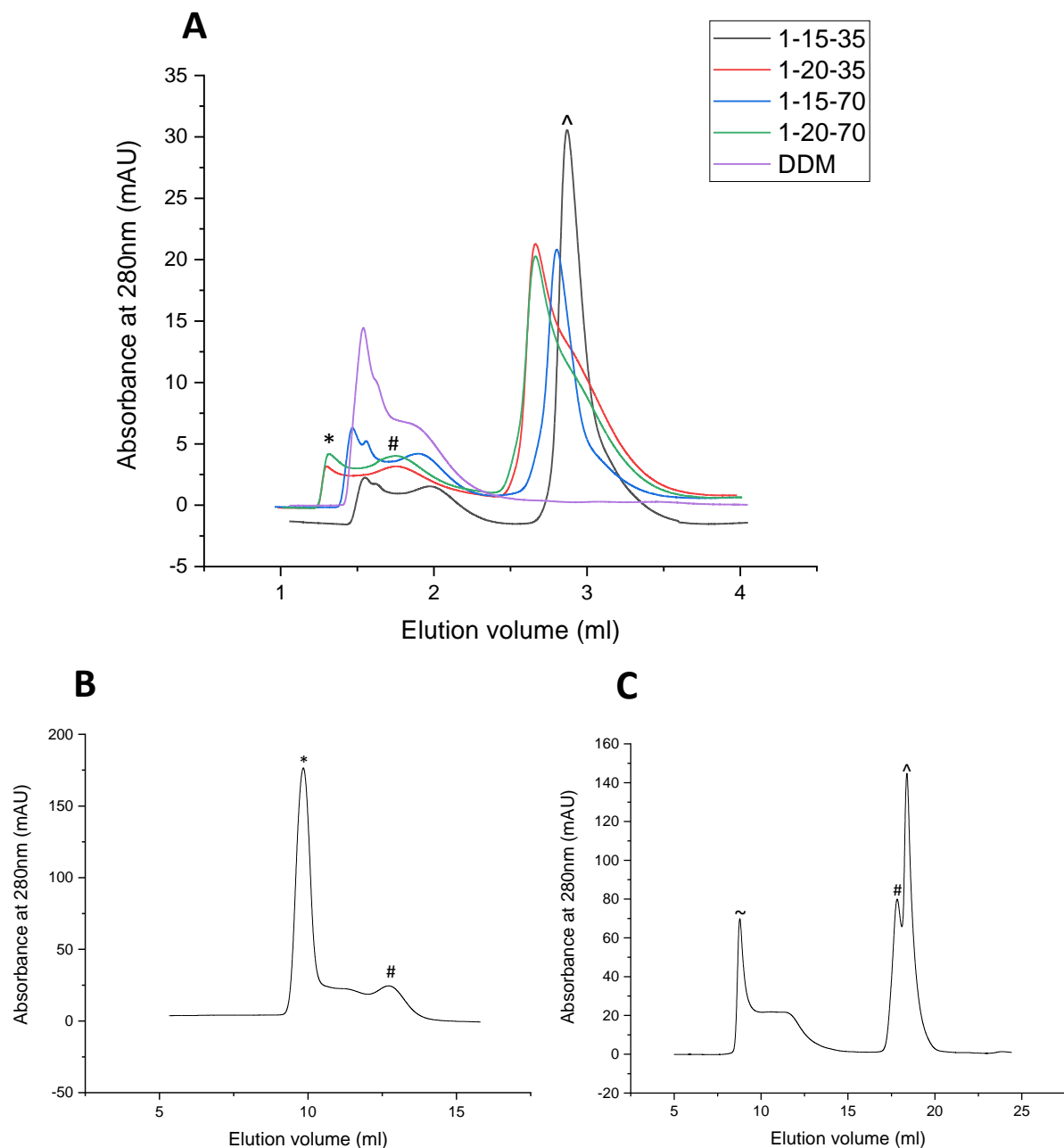


Figure 5: Reconstitution optimisation of MscM in SapA nanodiscs.

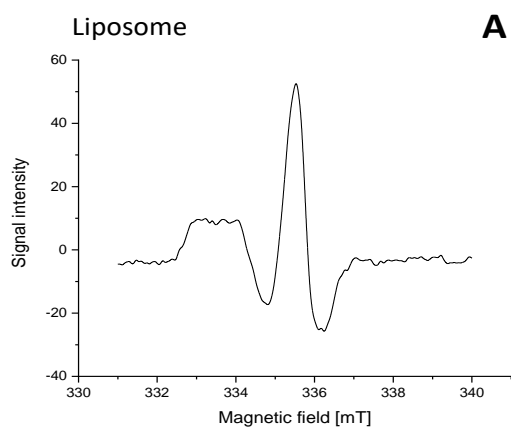
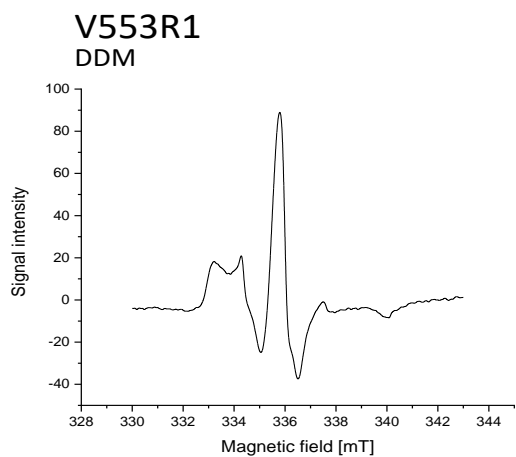
Reconstitution optimisation gel filtration profiles for the various MscM:SapA:SoyPC molar ratios used for the reconstitution are colour coded as indicated (A). Reconstitution of MscM in SapA nanodiscs before optimisation using molar ratio 1:15:35 (B). Reconstitution of MscM in SapA nanodiscs after optimisation using molar ratio 1:20:70 (C). Peak of soluble aggregates is marked with (~), free SapA is marked with (^), reconstituted MscM with (#) and MscM aggregation with (*). The elution volumes differ for the profiles due to the use of different size Superose6 columns, based on volume of preparation.

3.1.6 Liposome reconstitution

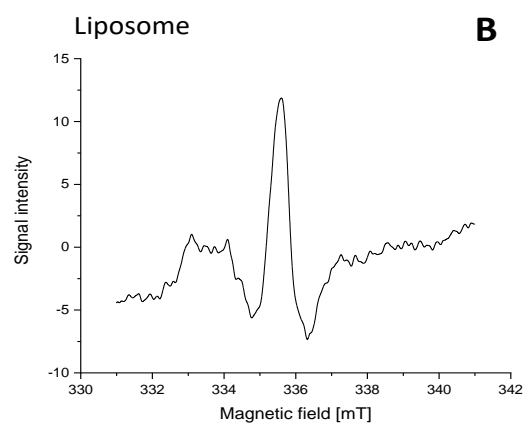
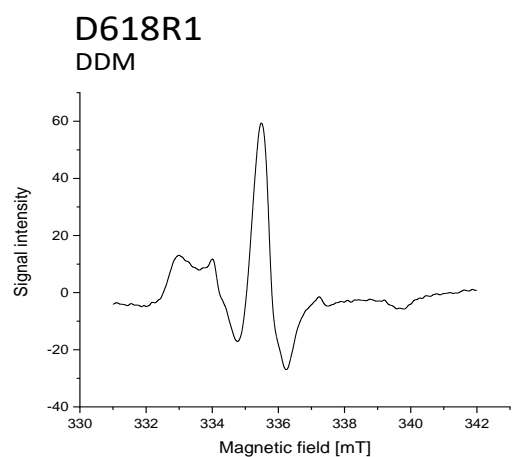
MscM reconstitution in liposomes was subsequently attempted. As the focus of the project was creating a lipid environment to embed MscM within, the morphology of the system was not a main issue of concern. The first sample, MscM V553R1 was reconstituted in SoyPC liposomes to produce a dense, white pellet and a corresponding cwEPR signal intensity of 50 (Fig. 6A). Three other external transmembrane helix mutants (D618C, K464C, L477C) were reconstituted using an identical protocol, but contrary to the reconstitution experiment results of V553R1, a visible pellet was not formed and consequently produced poor quality of cwEPR spectra (Fig. 6). The signal intensity was low in samples (Fig. 6B, 6C, 6D) resulting in noisy cwEPR spectra. All the DDM samples prior to reconstitution had protein concentrations between ~3-6 mg/mL. The reconstituted samples had concentrations between ~2-4 mg/mL prior to cwEPR measurement. The DDM sample for R737R1 was prepared previously by Dr Andrew Hartley, Pliotas Lab (Fig. 7A). Subsequently, the reconstitution experiment of R737R1, produced a thinner, pale-yellow pellet and a corresponding cwEPR signal of 23 (Fig. 7B). A higher cwEPR signal intensity was expected for this reconstitution, as it was a larger reconstitution, and the reconstituted sample concentration was higher than the previous samples at 11.93 mg/mL. In conclusion, the results of the liposome reconstitution experiments were inconsistent and require further investigation into the correlation between reconstitution pellet formation and good spin-labelling efficiency.

Studies have shown MS channels reconstituted in liposomes retain their function [73]. However, membrane protein orientation during liposomal reconstitution has been a factor that has been difficult to predict and influence. During a single reconstitution, hundreds of proteoliposomes are created, leading to significant heterogeneity [74]. Future implications of this project could include identifying a suitable lipid bilayer system where membrane protein orientation could be monitored, and possibly minimise molecular crowding. Molecular crowding is a shortcoming seen while using liposome-embedded proteins for PELDOR studies, spin label's phase memory time is shortened, this is a limitation for multispin labelled systems [72]. Employing appropriate stoichiometric ratios to ensure proper reconstitution yield in SapA nanodiscs and comparing PELDOR data of MscM within liposomal bilayer and SapA nanodiscs would be an interesting path to illuminate.

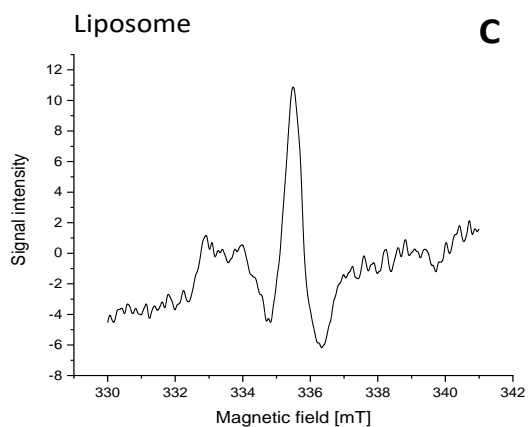
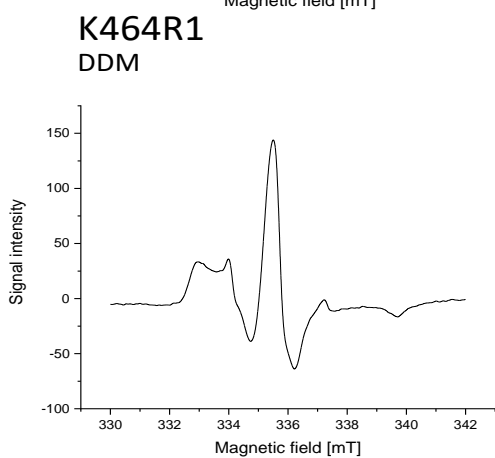
NP have been identified in structures of MscS probed by EPR in detergent and in bilayers. Within the NP, densities other than protein structures have been observed in cryo-EM structures as well as MD simulations. The densities have been identified as phospholipid molecules and their orientations and positions within the protein complex have been studied [2] [17]. MD simulations have shown that lipids within the NP are dynamic and continuously exchange. The cytoplasmic membrane leaflet was seen to supply the lipids to the NP more readily [2]. Rasmussen et al. reported three phospholipid molecules per subunit with cryoEM and that there are energetically favourable hydrophobic environments that allow lipid movements to approach the pockets [17].



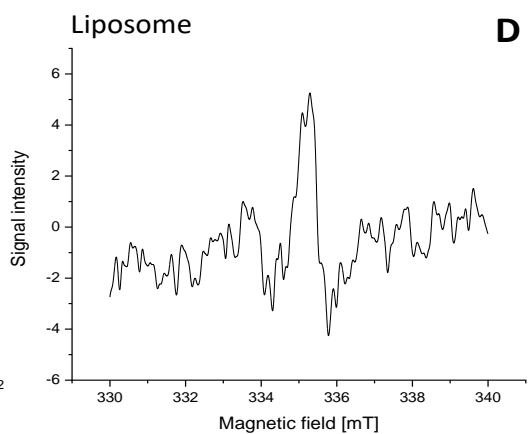
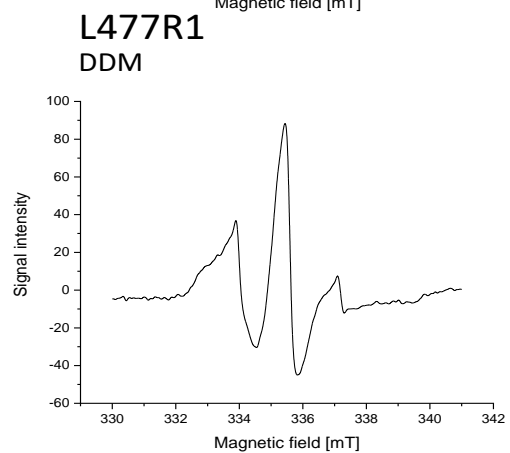
A



B



C



D

Figure 6: cwEPR spectra of MscM mutants in two conditions- DDM and in liposome. All samples were recorded at 4°C except for mutant MscM L477R1, which were completed at room temperature.

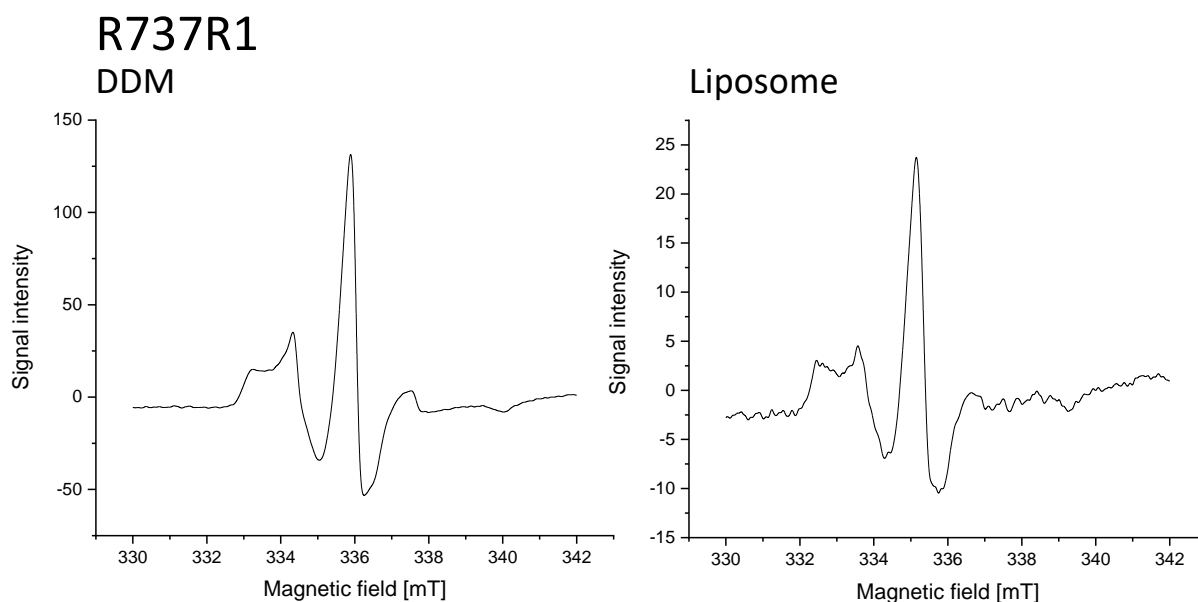


Figure 7: cwEPR spectra of MscM R737R1 in two conditions- DDM and in liposome. DDM sample was prepared and cwEPR measurements were done by Dr Andrew Hartley, Pliotas Lab.

3.2 MscS in MSP1E3D1 nanodisc

Previous studies have shown lipids trapped within MscS pockets using protein embedded lipid bilayer simulations. NP play a significant role in protein-lipid dynamics and hence, the conformational state of the protein [2]. The densities of lipids within pockets were observed in maps of MscS and were seen to decrease in different conformational states. They reported an average pocket lipid occupancy in different conformational states, closed state of MscS was seen to have ~3.3 lipids, open state had ~1.5 lipids and the subconducting state had 0.6 lipids [33]. To investigate lipid-protein dynamics, a 20 μ s coarse-grained molecular dynamics (CG-MD) simulation of the closed state of MscS (PDB:6RLD) in an MSP1E3D1 nanodisc with 184 1,2-dioleoyl-sn-glycero-3-phosphocholine (DOPC) was performed (Fig. 8). Residue 67 was considered the spin label as the simulation was coarse-grained and lacked the atomistic level of detail to

introduce a spin label at the site of interest. The 67th residue on the CG-MD simulation used as reference was a Leucine side chain bead. Lipid dynamics around the protein was observed over the course of 20 μ s, two acyl chains represent one lipid molecule (Fig. 9B). The labelled regions of the acyl chain (Fig. 9B) were used as reference to observe movement of the lipids. The number of acyl chains within 15Å of L67 during the span of 20 μ s was calculated. The simulation showed an average of 41 out of 386, ~11% of DOPC acyl chains in the nanodisc were within 15Å of L67 (Fig. 9A).

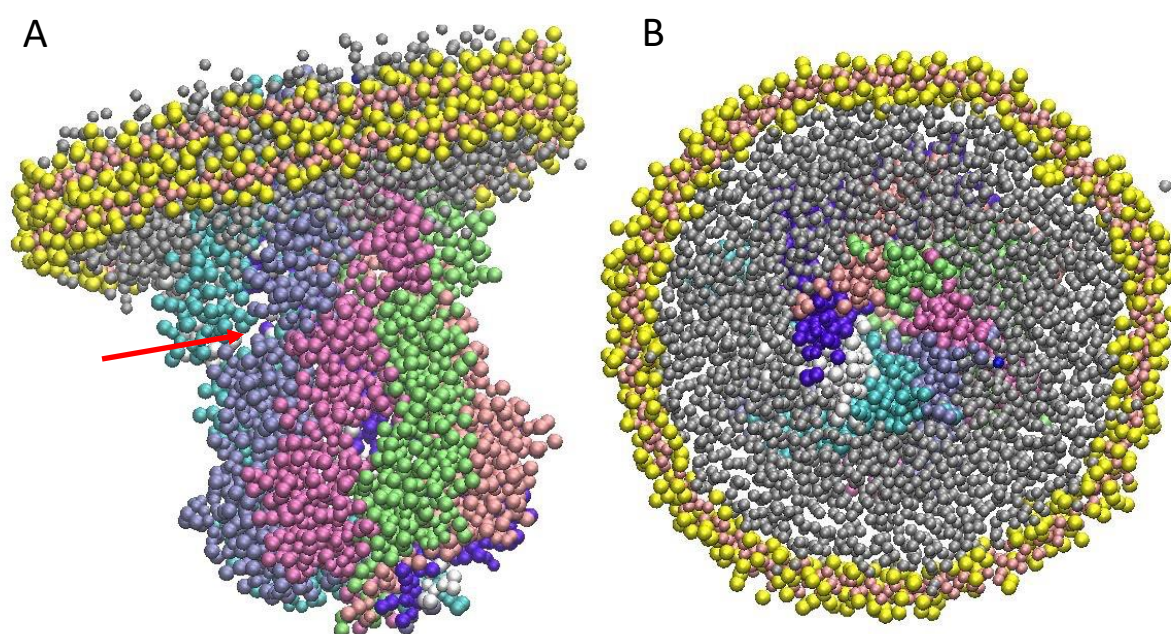


Figure 8: CG-MD simulation of MscS in MSP1E3D1 nanodisc and DOPC lipids.

The MscS-MSP1E3D1 nanodisc is represented by the yellow circular belt surrounding the DOPC molecules (grey beads) and MscS (multicoloured structure). Side view (A) and top view (B) of MscS within the nanodisc. The red arrow points at a nanopocket (NP) of MscS.

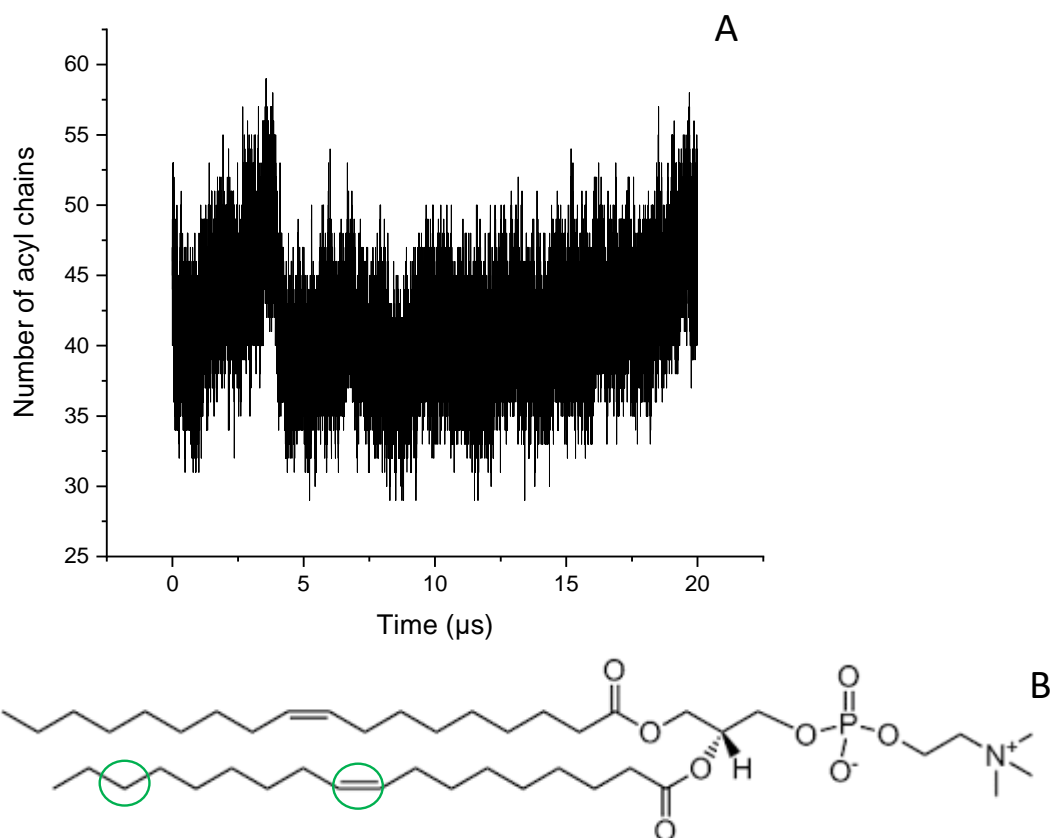


Figure 9: Number of acyl chains within 15Å of L67 of MscS within 20μs (A). The double bond region was used as the reference point of the lipid molecules to conduct the calculation (B).

To investigate lipid dynamics further and validate simulation analysis results, time spent by both double bond and terminal CH₃ regions of the acyl chains was calculated. The distribution of acyl chains based on the time spent within 15Å (Fig. 10A, 10B) was classified into three lipid dynamics categories. Acyl chains that were within 15Å for more than 8μs were broadly classified as trapped, between 5-8μs as intermediate, and less than 5μs as mobile lipids. The broad cut-off resulted in 22 trapped acyl chains (11 DOPC molecules) and 22 intermediate acyl chains (11 DOPC molecules). The indices of the calculations using both the double bond region and the CH₃ region corresponded to the same DOPC molecule, providing validation to the results of the analysis.

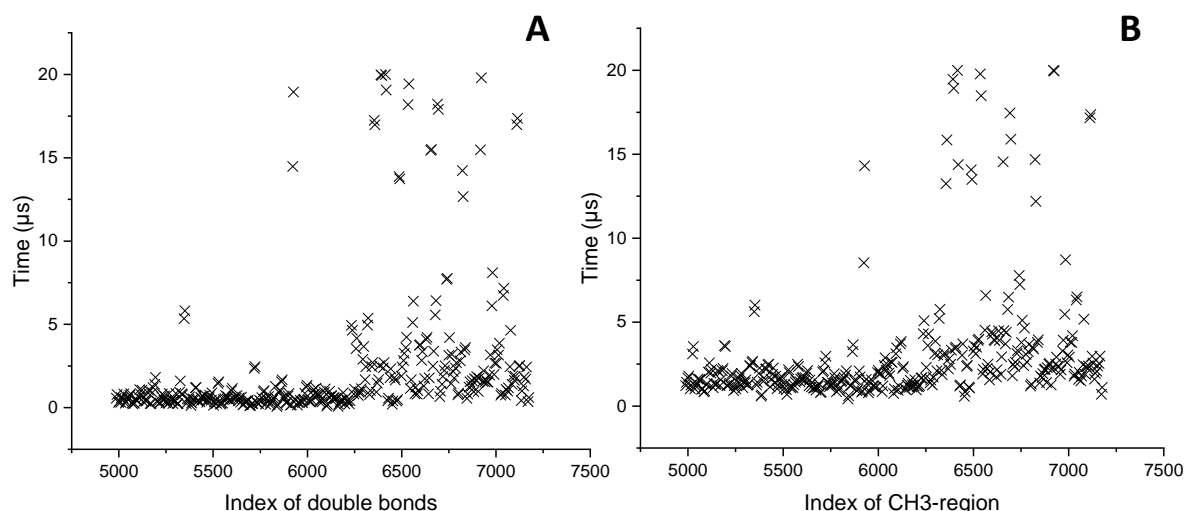


Figure 10: Scatter plot of the time spent by lipid acyl chains within 15Å of L67 over 20μs. Each x represents a unique index of the acyl chain. The indices shown in (A) represent the double bond regions of acyl chains, whereas indices in (B) represent the terminal CH₃ region.

Wang et al., observed on bilayer tension application, pocket lipids would orient more horizontally, with reference to the bulk bilayer lipids. Additionally, the study reported to enter or exit pockets, lipids should employ specific angles with relation to the membrane plane [34]. To further investigate the orientation and movement of acyl chains within the ‘trapped’ lipids category, the movement of acyl chains in this category was analysed. Analysis showed different dynamics of the two tails of a single DOPC molecule (Fig. 11). Six representative DOPC molecules out of eleven of the ‘trapped’ category are shown in Fig. 11. This result corresponds to results previous studies where acyl chains were seen to partially occupy NP of MS channels [2].

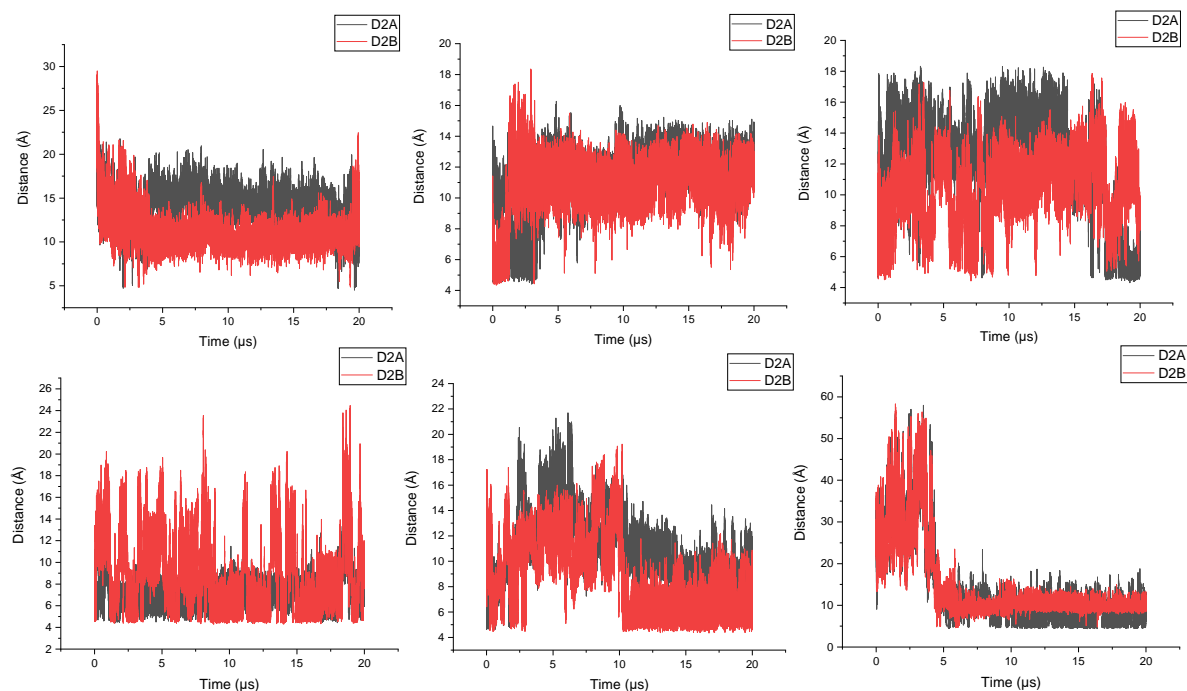


Figure 11: Trapped lipid acyl chains movement over 20 μ s. Each graph represents a trapped DOPC molecule. The red and grey traces represent each acyl chain of a DOPC molecule. D2A and D2B represent the double bond region on each acyl chain.

To observe the acyl chain occupancy in the NP, pocket-lining residues in the CG-MD simulation were identified. Subsequently, the average number of acyl chains within 5Å from a residue lining a NP of MscS (Fig. 8) over 20 μ s was calculated. An average of ~ 1.5 acyl chains (0.75 DOPC molecules) were seen over the course of the simulation; this fractionated number could be supported by the large distinction in dynamics between the two acyl chains (Fig. 11). As previously mentioned, the number of lipids seen in the subconducting state were ~ 0.6 lipids [33]. Further investigation would be required to observe global structural changes of the protein to the subconducting state.

Conclusion

Further experiments of the MscM project conducted by collaborators and members of the Piotas Lab, would include PELDOR and MD simulation experiments. In the scope of this project, since the application of cryoEM— powerful technique used to resolve protein structures, was unable to resolve MscM structure, PELDOR was adopted. PELDOR can be applied to give long-range restraints and observe the conformational state of the large protein complex of MscM when the use of other state-of-art techniques is challenging [75]. PELDOR distance distributions are the key results and data in this project, they would be used to computationally simulate MscM AlphaFold model in DDM and in lipid environment. PELDOR data can be utilised to probe function, set experimental constraints on models and to observe changes in secondary structure of MscM [12] [40]. The structure of MscM is unknown and using PELDOR to identify a conformational state in DDM and subsequently, in native lipid environment would be a significant step towards unravelling the structure of MscM. Within DDM, MscS from the MscS-like family, was seen to have consistent conformational states in crystal structure and in solution from PELDOR data. PELDOR data could give precise data of the separation of the transmembrane helices [12]. In this project, liposome reconstitution was done for mutants on the external helices of MscM; if there are structural changes in the protein that alter transmembrane helices between detergent and lipid environments, they can be detected using PELDOR. It is important to mention that MscS is a heptamer of 210 kDa. The use of PELDOR to probe the structure of MscM, a much larger and complex system of 900 kDa, is more challenging especially due to the lack of a previously resolved structural reference. Thus, the use of computational modelling goes hand in hand with the PELDOR data. This could be a novel diversified pathway using a cocktail of state-of-art techniques, to resolve structures of membrane proteins. Future implications for the MD simulations of this project would be to calculate lipid lateral diffusion, as this could be correlated with NMR data. With NMR, lipid diffusion rates have been calculated [76] and could be applied to identify lipid exchange rates between bulk bilayer and pockets.

References:

1. Martinac, B., *Mechanosensitive ion channels: molecules of mechanotransduction*. Journal of Cell Science, 2004. **117**(12): p. 2449-2460.
2. Pliotas, C., et al., *The role of lipids in mechanosensation*. Nature Structural & Molecular Biology, 2015. **22**(12): p. 991-998.
3. Hamill, O.P. and B. Martinac, *Molecular basis of mechanotransduction in living cells*. Physiol Rev, 2001. **81**(2): p. 685-740.
4. Hamilton, E.S., A.M. Schlegel, and E.S. Haswell, *United in diversity: mechanosensitive ion channels in plants*. Annu Rev Plant Biol, 2015. **66**: p. 113-37.
5. Basu, D. and E.S. Haswell, *Plant mechanosensitive ion channels: an ocean of possibilities*. Curr Opin Plant Biol, 2017. **40**: p. 43-48.
6. Nakayama, Y., K. Yoshimura, and H. Iida, *Organellar mechanosensitive channels in fission yeast regulate the hypo-osmotic shock response*. Nat Commun, 2012. **3**: p. 1020.
7. Dionysopoulou, M., et al., *Genetic and cellular characterization of MscS-like putative channels in the filamentous fungus Aspergillus nidulans*. Channels (Austin), 2022. **16**(1): p. 148-158.
8. Sukharev, S.I., et al., *Two types of mechanosensitive channels in the Escherichia coli cell envelope: solubilization and functional reconstitution*. Biophys J, 1993. **65**(1): p. 177-83.
9. Berrier, C., et al., *Multiple mechanosensitive ion channels from Escherichia coli, activated at different thresholds of applied pressure*. J Membr Biol, 1996. **151**(2): p. 175-87.

10. Edwards, M.D., et al., *Characterization of three novel mechanosensitive channel activities in Escherichia coli*. Channels (Austin), 2012. **6**(4): p. 272-81.
11. Schleyer, M., R. Schmid, and E.P. Bakker, *Transient, specific and extremely rapid release of osmolytes from growing cells of Escherichia coli K-12 exposed to hypoosmotic shock*. Arch Microbiol, 1993. **160**(6): p. 424-31.
12. Pliotas, C., et al., *Conformational state of the MscS mechanosensitive channel in solution revealed by pulsed electron–electron double resonance (PELDOR) spectroscopy*. Proceedings of the National Academy of Sciences, 2012. **109**(40): p. E2675.
13. Flegler, V.J., et al., *The MscS-like channel Ynal has a gating mechanism based on flexible pore helices*. Proc Natl Acad Sci U S A, 2020. **117**(46): p. 28754-28762.
14. Li, Y., et al., *Ionic regulation of MscK, a mechanosensitive channel from Escherichia coli*. The EMBO journal, 2002. **21**(20): p. 5323-5330.
15. Schumann, U., et al., *YbdG in Escherichia coli is a threshold-setting mechanosensitive channel with MscM activity*. Proc Natl Acad Sci U S A, 2010. **107**(28): p. 12664-9.
16. Reddy, B., et al., *Molecular basis of force-from-lipids gating in the mechanosensitive channel MscS*. eLife, 2019. **8**: p. e50486.
17. Rasmussen, T., et al., *Structure of the Mechanosensitive Channel MscS Embedded in the Membrane Bilayer*. J Mol Biol, 2019. **431**(17): p. 3081-3090.
18. Bass, R.B., et al., *Crystal structure of Escherichia coli MscS, a voltage-modulated and mechanosensitive channel*. Science, 2002. **298**(5598): p. 1582-7.
19. Sukharev, S.I., et al., *A large-conductance mechanosensitive channel in E. coli encoded by mscL alone*. Nature, 1994. **368**(6468): p. 265-8.

20. Pliotas, C. and J.H. Naismith, *Spectator no more, the role of the membrane in regulating ion channel function*. Current Opinion in Structural Biology, 2017. **45**: p. 59-66.
21. Li, J., et al., *Mechanical coupling of the multiple structural elements of the large-conductance mechanosensitive channel during expansion*. Proceedings of the National Academy of Sciences, 2015. **112**(34): p. 10726-10731.
22. Kapsalis, C., et al., *In-Lipid Structure of Pressure-Sensitive Domains Hints Mechanosensitive Channel Functional Diversity*. Biophysical Journal, 2020. **119**(2): p. 448-459.
23. Blount, P., et al., *Single residue substitutions that change the gating properties of a mechanosensitive channel in Escherichia coli*. Proceedings of the National Academy of Sciences, 1996. **93**(21): p. 11652.
24. Bavi, N., et al., *The role of MscL amphipathic N terminus indicates a blueprint for bilayer-mediated gating of mechanosensitive channels*. Nature Communications, 2016. **7**(1): p. 11984.
25. D'Alessandro, B., et al., *Comparative genomics of Salmonella enterica serovar Enteritidis ST-11 isolated in Uruguay reveals lineages associated with particular epidemiological traits*. Scientific Reports, 2020. **10**(1): p. 3638.
26. Wang, Y., et al., *Comparative Genomic Analysis and Characterization of Two Salmonella enterica Seroovar Enteritidis Isolates From Poultry With Notably Different Survival Abilities in Egg Whites*. Frontiers in Microbiology, 2018. **9**.
27. Gu, Y. and C. Gu, *Physiological and pathological functions of mechanosensitive ion channels*. Mol Neurobiol, 2014. **50**(2): p. 339-47.
28. Michalick, L. and W.M. Kuebler, *TRPV4-A Missing Link Between Mechanosensation and Immunity*. Frontiers in immunology, 2020. **11**: p. 413-413.

29. Liedtke, W. and J.M. Friedman, *Abnormal osmotic regulation in trpv4^{-/-} mice*. Proceedings of the National Academy of Sciences, 2003. **100**(23): p. 13698-13703.
30. Jojoa-Cruz, S., et al., *Structural insights into the Venus flytrap mechanosensitive ion channel Flycatcher1*. Nature Communications, 2022. **13**(1): p. 850.
31. Martinac, B., J. Adler, and C. Kung, *Mechanosensitive ion channels of E. coli activated by amphipaths*. Nature, 1990. **348**(6298): p. 261-263.
32. Rasmussen, T., et al., *Interaction of the Mechanosensitive Channel, MscS, with the Membrane Bilayer through Lipid Intercalation into Grooves and Pockets*. Journal of Molecular Biology, 2019. **431**(17): p. 3339-3352.
33. Zhang, Y., et al., *Visualization of the mechanosensitive ion channel MscS under membrane tension*. Nature, 2021. **590**(7846): p. 509-514.
34. Wang, B., et al., *Pocket delipidation induced by membrane tension or modification leads to a structurally analogous mechanosensitive channel state*. Structure, 2022. **30**(4): p. 608-622.e5.
35. Cahalan, S.M., et al., *Piezo1 links mechanical forces to red blood cell volume*. eLife, 2015. **4**: p. e07370.
36. Saotome, K., et al., *Structure of the mechanically activated ion channel Piezo1*. Nature, 2018. **554**(7693): p. 481-486.
37. Wang, L., et al., *Structure and mechanogating of the mammalian tactile channel PIEZO2*. Nature, 2019. **573**(7773): p. 225-229.
38. Sahu, I.D. and G.A. Lorigan, *Electron Paramagnetic Resonance as a Tool for Studying Membrane Proteins*. Biomolecules, 2020. **10**(5): p. 763.

39. Joseph, B., et al., *In situ observation of conformational dynamics and protein ligand–substrate interactions in outer-membrane proteins with DEER/PELDOR spectroscopy*. Nature Protocols, 2019. **14**(8): p. 2344-2369.
40. Hartley, A.M., et al., *Using pulsed EPR in the structural analysis of integral membrane proteins*, in *Electron Paramagnetic Resonance: Volume 27*. 2021, The Royal Society of Chemistry. p. 74-108.
41. Ackermann, K., et al., *Sparse Labeling PELDOR Spectroscopy on Multimeric Mechanosensitive Membrane Channels*. Biophys J, 2017. **113**(9): p. 1968-1978.
42. Howard, M.J., *Protein NMR spectroscopy*. Curr Biol, 1998. **8**(10): p. R331-3.
43. Opella, S.J. and F.M. Marassi, *Applications of NMR to membrane proteins*. Arch Biochem Biophys, 2017. **628**: p. 92-101.
44. Danmaliki, G.I. and P.M. Hwang, *Solution NMR spectroscopy of membrane proteins*. Biochim Biophys Acta Biomembr, 2020. **1862**(9): p. 183356.
45. Benjin, X. and L. Ling, *Developments, applications, and prospects of cryo-electron microscopy*. Protein science : a publication of the Protein Society, 2020. **29**(4): p. 872-882.
46. Renaud, J.-P., et al., *Cryo-EM in drug discovery: achievements, limitations and prospects*. Nature Reviews Drug Discovery, 2018. **17**(7): p. 471-492.
47. Kermani, A.A., *A guide to membrane protein X-ray crystallography*. Febs j, 2021. **288**(20): p. 5788-5804.
48. Smyth, M.S. and J.H. Martin, *x ray crystallography*. Molecular pathology : MP, 2000. **53**(1): p. 8-14.

49. Frick, M., C. Schwieger, and C. Schmidt, *Liposomes as Carriers of Membrane-Associated Proteins and Peptides for Mass Spectrometric Analysis*. Angewandte Chemie International Edition, 2021. **60**(20): p. 11523-11530.
50. Bayburt, T.H., Y.V. Grinkova, and S.G. Sligar, *Self-Assembly of Discoidal Phospholipid Bilayer Nanoparticles with Membrane Scaffold Proteins*. Nano Letters, 2002. **2**(8): p. 853-856.
51. Denisov, I.G., et al., *Directed Self-Assembly of Monodisperse Phospholipid Bilayer Nanodiscs with Controlled Size*. Journal of the American Chemical Society, 2004. **126**(11): p. 3477-3487.
52. Denisov, I.G. and S.G. Sligar, *Nanodiscs for structural and functional studies of membrane proteins*. Nature Structural & Molecular Biology, 2016. **23**(6): p. 481-486.
53. Puthenveetil, R. and O. Vinogradova, *Solution NMR: A powerful tool for structural and functional studies of membrane proteins in reconstituted environments*. J Biol Chem, 2019. **294**(44): p. 15914-15931.
54. Popovic, K., et al., *Structure of saposin A lipoprotein discs*. Proceedings of the National Academy of Sciences, 2012. **109**(8): p. 2908-2912.
55. Jumper, J., et al., *Highly accurate protein structure prediction with AlphaFold*. Nature, 2021. **596**(7873): p. 583-589.
56. Hollingsworth, S.A. and R.O. Dror, *Molecular Dynamics Simulation for All*. Neuron, 2018. **99**(6): p. 1129-1143.
57. Bennett, W.F. and D.P. Tieleman, *Computer simulations of lipid membrane domains*. Biochim Biophys Acta, 2013. **1828**(8): p. 1765-76.

58. Corey, R.A., et al., *Insights into Membrane Protein–Lipid Interactions from Free Energy Calculations*. Journal of Chemical Theory and Computation, 2019. **15**(10): p. 5727-5736.
59. Kmiecik, S., et al., *Coarse-Grained Protein Models and Their Applications*. Chemical Reviews, 2016. **116**(14): p. 7898-7936.
60. Bradley, R. and R. Radhakrishnan, *Coarse-Grained Models for Protein-Cell Membrane Interactions*. Polymers, 2013. **5**(3).
61. Delano W, L., *The PyMOL Molecular Graphics System*. <http://www.pymol.org>, 2002.
62. Humphrey, W., A. Dalke, and K. Schulten, *VMD: visual molecular dynamics*. J Mol Graph, 1996. **14**(1): p. 33-8, 27-8.
63. Jo, S., et al., *CHARMM-GUI: A web-based graphical user interface for CHARMM*. Journal of Computational Chemistry, 2008. **29**(11): p. 1859-1865.
64. Abraham, M.J., et al., *GROMACS: High performance molecular simulations through multi-level parallelism from laptops to supercomputers*. SoftwareX, 2015. **1-2**: p. 19-25.
65. Pliotas, C., *Chapter Eight - Ion Channel Conformation and Oligomerization Assessment by Site-Directed Spin Labeling and Pulsed-EPR*, in *Methods in Enzymology*, C. Ziegler, Editor. 2017, Academic Press. p. 203-242.
66. Lane, B.J., et al., *HDX-guided EPR spectroscopy to interrogate membrane protein dynamics*. STAR Protocols, 2022. **3**(3): p. 101562.
67. Flayhan, A., et al., *Saposin Lipid Nanoparticles: A Highly Versatile and Modular Tool for Membrane Protein Research*. Structure, 2018. **26**(2): p. 345-355.e5.

68. Kapsalis, C., et al., *Allosteric activation of an ion channel triggered by modification of mechanosensitive nano-pockets*. Nature Communications, 2019. **10**(1): p. 4619.
69. Flegler, V.J., et al., *Mechanosensitive channel gating by delipidation*. Proceedings of the National Academy of Sciences, 2021. **118**(33): p. e2107095118.
70. Bornhorst, J.A. and J.J. Falke, [16] *Purification of proteins using polyhistidine affinity tags*, in *Methods in Enzymology*. 2000, Academic Press. p. 245-254.
71. Georgieva, E.R., *Protein Conformational Dynamics upon Association with the Surfaces of Lipid Membranes and Engineered Nanoparticles: Insights from Electron Paramagnetic Resonance Spectroscopy*. Molecules, 2020. **25**(22): p. 5393.
72. Ward, R., et al., *Probing the Structure of the Mechanosensitive Channel of Small Conductance in Lipid Bilayers with Pulsed Electron-Electron Double Resonance*. Biophysical Journal, 2014. **106**(4): p. 834-842.
73. Sukharev, S., *Purification of the Small Mechanosensitive Channel of Escherichia coli (MscS): the Subunit Structure, Conduction, and Gating Characteristics in Liposomes*. Biophysical Journal, 2002. **83**(1): p. 290-298.
74. Amati, A.M., et al., *Current problems and future avenues in proteoliposome research*. Biochemical Society Transactions, 2020. **48**(4): p. 1473-1492.
75. Valera, S., et al., *Accurate Extraction of Nanometer Distances in Multimers by Pulse EPR*. Chemistry – A European Journal, 2016. **22**(14): p. 4700-4703.
76. Orädd, G. and G. Lindblom, *NMR Studies of Lipid Lateral Diffusion in the DMPC/Gramicidin D/Water System: Peptide Aggregation and Obstruction Effects*. Biophysical Journal, 2004. **87**(2): p. 980-987.

